Journal of Computational Physics 340 (2017) 688–711

Contents lists available at ScienceDirect

Journal of Computational Physics

www.elsevier.com/locate/jcp

Fluid–particle dynamics for passive tracers advected by a thermally fluctuating viscoelastic medium

Christel Hohenegger [a,*], Scott A. McKinley [b,1]

[a] Department of Mathematics, The University of Utah, 155 S 1400 E Room 233, Salt Lake City, UT 84112-0090, United States
[b] Department of Mathematics, Tulane University, 6823 St. Charles Ave, New Orleans, LA 70118, United States

ARTICLE INFO

Article history:
Received 20 May 2016
Received in revised form 23 January 2017
Accepted 27 March 2017
Available online 7 April 2017

Keywords:
Anomalous diffusion
Viscoelastic fluid
Stochastic process

ABSTRACT

Many biological fluids, like mucus and cytoplasm, have prominent viscoelastic properties. As a consequence, immersed particles exhibit *subdiffusive* behavior, which is to say, the variance of the particle displacement grows sublinearly with time. In this work, we propose a viscoelastic generalization of the Landau–Lifschitz Navier–Stokes fluid model and investigate the properties of particles that are passively advected by such a medium. We exploit certain exact formulations that arise from the Gaussian nature of the fluid model and introduce analysis of memory in the fluid statistics, marking an important step toward capturing fluctuating hydrodynamics among subdiffusive particles. The proposed method is spectral, meshless and is based on the numerical evaluation of the covariance matrix associated with individual fluid modes. With this method, we probe a central hypothesis of *passive microrheology*, a field premised on the idea that the statistics of particle trajectories can reveal fundamental information about their surrounding fluid environment.

1. Introduction

Many fundamental biological processes concern the movement of microparticles in complex fluids – that is, liquids that contain suspended polymers, microbes, or other microstructures. For example, mucus is a suspension of oligomeric mucin proteins in a water-like fluid and whole blood is a suspension of red blood cells in plasma. Complex fluids are noted for the wide variety of mechanical responses they exhibit as a function of applied strain/stress. In response to certain stimuli, a complex fluid will act like a solid, but in response to other stimuli, the same fluid will act like a liquid. These viscoelastic rheological properties are often caused by interactions between suspended microstructures and a viscous background fluid [1–4].

Particles diffusing in viscous fluids act like classical Brownian motion, but particles moving in viscoelastic fluids tend to be statistically distinct, exhibiting the effects of memory and long-range particle–particle correlation. Indeed the motion of foreign microparticles in complex fluids is very rarely well-described by classical Brownian motion. The primary statistical tool used in particle tracking analysis is mean-squared displacement (MSD), the empirical second moment of change in particle position. For particles moving in a purely viscous fluid, the MSD grows linearly with time; while, in viscoelastic media, the MSD scales nonlinearly. Recent interest in material properties of biological fluids has led to the cataloguing of numerous natural examples of this so-called *anomalous diffusion*. For a few examples, see [5–9].

* Corresponding author.
E-mail addresses: choheneg@math.utah.edu (C. Hohenegger), scott.mckinley@tulane.edu (S.A. McKinley).
[1] Previously affiliated with University of Florida, Department of Mathematics, Gainesville, FL.

http://dx.doi.org/10.1016/j.jcp.2017.03.053
0021-9991/

The widespread observation of anomalous diffusion in complex fluids has led to the development of several mathematical models that have been variously successful in describing the paths of individual particles. For example, it was recently demonstrated that the motion of 500 nm radius latex beads in human mucus is well-described by fractional Brownian motion (FBM) [10]. Subsequently it was shown that a force-balance approach to modeling, called the generalized Langevin equation (GLE), can provide an even more faithful model for the data [11].

However the extension of single-particle theory to that of multiple interacting particles remains elusive. FBM and GLE are characterized by anti-persistent memory effects (meaning that movement in one direction during one time step is positively correlated with movement in the opposite direction in the next) that result from the storage of energy and response by the surrounding viscoelastic medium. There is no doubt that the medium also communicates disturbances nonlocally across distances as well, and it stands to reason that two proximate particles should have nontrivial interactions with each other. While there exist mathematical frameworks that might have the potential to do so (see complex fluid models like [12] and [13] for example), we know of no work that shows immersed particles behaving as FBM or GLE when alone, but when nearby each other, interacting through fluctuating hydrodynamics. In this article, we take a step in this direction by developing a modeling and simulation framework for particles that are passively advected by a linear viscoelastic fluid.

Because our fluid–particle model will require the interaction of forces, we adopt a GLE approach. The GLE is a stochastic integro-differential equation that was introduced by Kubo [14] and then revived for the purpose of modeling viscoelastic diffusion by Mason and Weitz [15]. Here we adopt the following definition for the GLE, which describes the velocity $V(t)$ of a particle:

$$m\mathrm{d}V(t) = \Big(-\gamma_s V(t) - \frac{\gamma_p}{\tau}\int_{-\infty}^{t} K(t-s)V(s)\mathrm{d}s + \sqrt{\frac{k_B T\gamma_p}{\tau}}F(t)\Big)\mathrm{d}t + \sqrt{2k_B T\gamma_s}\,\mathrm{d}W(t). \tag{1}$$

When referring to the particle position, $X(t) = \int_0^t V(s)\mathrm{d}s$, we say that X satisfies the integrated GLE (iGLE). The GLE (1) is a balance of forces equation relating the particle's acceleration to its velocity history and to thermal fluctuations in the fluid environment. Here, m is the particle's mass, k_B is Boltzmann constant and T is the temperature. The force of friction is decomposed into two components: the drag due to solvent viscosity γ_s and drag due to the polymeric component of the fluid environment, comprised of a memory kernel $K(t)$, a leading drag coefficient γ_p, and a normalizing constant $\tau = \int_0^\infty K(s)\mathrm{d}s$ that has units of $[\mathtt{time}]$. The memory kernel K summarizes the fluid environment's capacity to store energy and act back on a particle after a given increment of time. For discussion on the inclusion of instantaneous viscous response term see [16]. The force due to thermal fluctuations is also decomposed into solvent and polymeric component contributions. The term $W(t)$ is a standard Brownian motion, while $F(t)$ is a stationary Gaussian process with mean 0 and autocovariance given by

$$\mathbb{E}[F(t)F(s)] = K(t-s). \tag{2}$$

This form for the noise is posited in accordance with the *fluctuation–dissipation* relationship [14]. In Section 2, we establish some basic facts about the GLE, including a discussion of our choice for the memory kernel K and our method of simulation.

Initial efforts to model the interaction of multiple particles used a system of GLEs with an interaction term meant to summarize the hydrodynamic influence of one particle on the other [17–20]. However, when implementing the noise terms, these methods tended to ignore correlations that exist with past position and velocity. In particular, there is disagreement about how to enforce the fluctuation–dissipation relationship among multiple beads and through the background fluid without directly modeling the fluid velocity field as well. For this reason it is appealing to note recent developments in numerical fluid–particle coupling methods [12,21–23]. When considering neutrally buoyant particles in an incompressible fluid, the stochastic Immersed Boundary Method has been particularly successful in capturing statistical properties of particle trajectories in viscous fluids [24–28]. In this work, we present an important step toward implementing the stochastic IBM for *viscoelastic* fluids: generalizing the fluctuating Landau–Lifschitz Navier–Stokes equations for viscoelastic fluids and simulating trajectories of passively advected immersed particles.

In Section 3 we develop our model for the fluid velocity field $\mathbf{u}$ and explore the challenges that exist in generating efficient and accurate simulations. The main difficulty arises from two key issues. The first is that, unlike the stochastic IBM for viscous fluids, which can employ step-by-step simulation techniques exploiting the Markov property, the primary tool available for our model is the theory of stationary Gaussian processes. While conceptually straightforward, the implementation presents many practical problems, mostly stemming from our second challenge: that the physical regime of interest corresponds to a situation where the memory kernel has a very slow (power law) decay. As explained in the next section, we use a memory kernel whose form is a sum of exponential functions. The "more viscoelastic" a fluid is, the more terms are necessary in the sum, in turn complicating calculations involving the temporal Fourier transform.

For a neutrally buoyant particle, we consider the equation of motion to be given by averaging over a small region of the fluid velocity field $\mathbf{u}(\mathbf{x},t)$ centered at the particle location:

$$\frac{\mathrm{d}\mathbf{X}(t)}{\mathrm{d}t} = \int \delta_a(\mathbf{x}-\mathbf{X}(t))\mathbf{u}(\mathbf{x},t)\mathrm{d}\mathbf{x}. \tag{3}$$

Here, δ_a is an approximate delta-function with characteristic length scale a chosen following standard IBM techniques. In Section 4, we provide the details of the semi-Euler method we use to generate particle paths.

In Sections 5 we explore the behavior of the model through a combination of mathematical and numerical results. We start by recording some basic mathematical results and demonstrate numerical convergence of our simulation method. After introducing physically appropriate parameter choices we analyze the fluid–particle relationship in detail.

One major motivation for this work is to investigate the assumptions underlying an important subfield of particle tracking research called *passive microrheology*. The premise of the field is that the statistics of particle trajectories can be used to recover defining properties of the surrounding viscoelastic fluid [29–31]. We therefore explicitly analyze the output of our model in terms of the two major summary statistics used in the experimental particle tracking literature: the particle MSD and the auto-correlation function (ACF) of the increments of the particle position process (see Section 5.4). For the system we present here, where particles are passively advected by the fluid environment, we find validation for these assumptions, and in Section 5.6 we document the critical features of the model that seem to make it possible.

2. Mathematical background: the generalized Langevin equation

In the modeling of viscoelastic diffusion, we encounter the GLE in two distinct contexts: first (as defined in the previous section) as a description of an individual particle's velocity process, and then second as a building block for our model of a viscoelastic fluid. Removing the physical meaning of the constants, we consider mean-zero stationary solutions to a GLE that has the following form: for $a \geq 0$, $b > 0$ and $c > 0$,

$$\mathrm{d}Y(t) = \left[-aY(t) - b(K^+ * Y)(t) + c\sqrt{b}F(t)\right]\mathrm{d}t + c\sqrt{2a}\mathrm{d}W(t) \tag{4}$$

where $W(t)$ is a standard Brownian motion and $F(t)$ is a mean-zero stationary Gaussian process with covariance function

$$\mathbb{E}[F(t)F(s)] = K(t-s). \tag{5}$$

In the above, we assume that $K \in L_1(\mathbb{R})$ is an even function; $K^+(t) := \mathbb{1}_{\{t\geq 0\}}(t)K(t)$, where $\mathbb{1}$ is the indicator function; and $*$ denotes convolution in time. Associated with (4) is the integrated process $Z(t)$ which is defined by pathwise integration. That is, the memory kernel K will be defined in such a way that, the process $\{Y(t;\omega)\}_{t\in\mathbb{R}}$ is continuous almost surely, and for each such ω,

$$Z(t;\omega) := \int_0^t Y(s;\omega)ds. \tag{6}$$

We say that a mean-zero, stationary, Gaussian process $\{Y(t)\}_{t\in\mathbb{R}}$ is a solution to the GLE if the Fourier transform of its covariance function $\rho_Y(t) = \mathbb{E}[Y(t)Y(0)]$ has the form

$$\widehat{\rho_Y}(\xi) = \frac{c^2(2a + b\hat{K}(\xi))}{|i\xi + a + b\widehat{K^+}(\xi)|^2}. \tag{7}$$

Here we take the following definition of the Fourier transform pair:

$$\hat{f}(\xi) = \int_{\mathbb{R}} f(t)e^{-i\xi t}\mathrm{d}t, \quad f(t) = \frac{1}{2\pi}\int_{\mathbb{R}} \hat{f}(\xi)e^{i\xi t}\mathrm{d}\xi.$$

See [32] for an example derivation of Eq. (7).

Following modeling choices made in [11,33,34], we consider memory kernels K of the form,

$$K(t) = \sum_{n=0}^{N-1} c_n e^{-|t|/\tau_n}, \tag{8}$$

where $\tau_0 < \tau_1 < \ldots < \tau_{N-1}$ are called relaxation times. The use of a superposition of linear responses at discrete time scales echoes results from polymer kinetic theory, especially of the Rouse polymer model [35]. Indeed, when $\tau_n = \tau_0(N/(N-n))^\alpha$ for some $\alpha > 1$ and the coefficients $c_n \equiv 1/N$, we say that $K(t)$ is a *generalized Rouse kernel*, and the case $\alpha = 2$ exhibits the same large-time MSD behavior as a single monomer in a Rouse chain [34]. As the number of terms in the exponential series increases, the large-t tail of $K(t)$ approximates the power law $t^{-1/\alpha}$ and the associated iGLE exhibits anomalous diffusive characteristics. Such a large N limit has also been computed, for example, in the derivation of the GLE from heat bath models [36,37]. There are a few advantages to writing the memory kernel as a sum of exponentials. First, the parameter N provides a way to interpolate seamlessly between essentially viscous dynamics ($N = 1$) and fully viscoelastic dynamics (N large). Second, in terms of regularity of solutions, it has previously been shown [33] that, by introducing auxiliary equations, the GLE with a sum-of-exponentials kernel can be rewritten as a linear high-dimensional system of SDEs driven by additive noise. It immediately follows that solutions exist and are almost surely continuous.

According to standard statistical mechanics, the coefficients of the one-dimensional GLE must be chosen so that the solution $Y(t)$ to (1) satisfies the kinetic energy constraint $\mathbb{E}\left[Y^2(0)\right] = k_B T/m$ for all $t \in \mathbb{R}$ [14]. In terms of the autocorrelation function (7), this is equivalent to requiring that

$$\frac{1}{2\pi}\int_{\mathbb{R}} \widehat{\rho_Y}(\xi)\mathrm{d}\xi = \frac{k_B T}{m}. \tag{9}$$

To compute the integral on the left-hand side, we introduce the following proposition.

Proposition 2.1. *Let $Y(t)$ be a Gaussian stationary solution to (4) with memory kernel $K(t)$ defined by (8). Then*

$$\mathbb{E}\left[Y^2(0)\right] = c^2. \tag{10}$$

The novelty of the result is that this holds regardless of the relaxation spectrum $\{\tau_n\}$ as long as $c_n \equiv 1/N$.

Proof. In what follows, we use the usual notation for a complex number z, denoting by $\mathrm{Re}(z)$ its real part, by $\mathrm{Im}(z)$ its imaginary part and by $\bar{z}$ its complex conjugate. Furthermore, $\mathrm{Res}(\Psi, \omega)$ is the residue of $\Psi(\xi)$ evaluated at ω. By construction,

$$\mathbb{E}\left[Y^2(0)\right] = \rho_Y(0) = \frac{1}{2\pi}\int_{\mathbb{R}} \widehat{\rho_Y}(\xi)\mathrm{d}\xi = \frac{1}{\pi}\int_0^\infty \widehat{\rho_Y}(\xi)\mathrm{d}\xi.$$

The proof is based on the results of [38], where we showed that for $a = 0$

$$\int_0^\infty \Psi(\xi)\mathrm{d}\xi = \pi$$

where $\widehat{\rho_Y}(\xi) = c^2\Psi(\xi)$. If $a \neq 0$, the steps are very similar and we sketch them here. First, we define the auxiliary function $\Psi(\xi)$ in the following way:

$$\Psi(\xi) = \frac{2a + 2b\mathrm{Re}(\Phi(i\xi))}{|i\xi + a + b\Phi(i\xi)|^2}, \text{ where } \Phi(x) = \frac{1}{N}\sum_{n=0}^{N-1}\frac{1}{x+\lambda_n},$$

and where $\lambda_n = \tau_n^{-1}$, $n = 0, \ldots, N-1$. The partial fraction decomposition of $\Psi(\xi)$ is

$$\Psi(\xi) = \frac{1}{i\xi + a + b\Phi(i\xi)} + \frac{1}{-i\xi + a + b\Phi(-i\xi)} = \frac{p(i\xi)}{q(i\xi)} + \frac{p(-i\xi)}{q(-i\xi)}.$$

In the above, the polynomials $p(x), q(x)$ are $p(x) = \prod_{n=0}^{N-1}(x+\lambda_n)$ and $q(x) = (x+a)p(x) + \frac{b}{N}p'(x)$, where $'$ denotes the derivative with respect to x. In [38] we showed that, if $a = 0$, then $\Psi(\xi)$ is even and $-z_n$, $n = 0, \ldots, N$ the roots of $q(x)$ are such that $z_n > 0$ for $n = 0, \ldots, N-2$ and $z_N = \overline{z_{N-1}}$ with $\mathrm{Re}(z_{N-1}) > 0$. The reasoning and the conclusions reached in [38] are the same if $0 < a < \lambda_N$ and they can be extended for all a.

Therefore, if we let $\omega_n = iz_n$, $n = 0, \ldots, N$, then the ω_n's are the roots of $q(i\omega)$ and they are located in the upper-half plane, more precisely $\omega_1, \ldots, \omega_{N-2} \in i\mathbb{R}^+$ and $\mathrm{Im}(\omega_{N-1,N}) > 0$. The roots of $q(-i\xi)$ are the complex conjugates of the roots of $q(i\xi)$ and we have $\overline{\omega_n} = -\omega_n$, $n = 0, \ldots, N-1$ and $\overline{\omega_{N-1,N}} = -\omega_{N,N-1}$. Using Vieta's formula and the series expansion of $p(i\xi), q(i\xi), p(-i\xi), q(-i\xi)$, one can show that the degree of the numerator of $\Psi(\xi)$ is $2N$ while the degree of the denominator is $2N+2$. Thus $\Psi(\xi)$ has proper decay at infinity to apply the residue theorem on a circular contour, which gives

$$\int_0^\infty \Psi(\xi)\mathrm{d}\xi = \frac{\pi i}{2}\sum_{n=0}^{N}\left[\mathrm{Res}(\Psi, \omega_n) - \mathrm{Res}(\Psi, \overline{\omega_n})\right].$$

Since $\mathrm{Res}(\Psi, \overline{\omega_n}) = -\mathrm{Res}(\Psi, \omega_n)$ for $n = 0, \ldots, N-2$ and $\mathrm{Res}(\Psi, \overline{\omega_{N-1,N}}) = -\mathrm{Res}(\Psi, \omega_{N,N-1})$, the above reduces to $\pi i \sum_{n=0}^{N}\mathrm{Res}(\Psi, \omega_n)$. Using the series expansion of $\Psi(\xi)$, we showed in [38] that the sum of the residues is $1/i$ yielding the desired equalities

$$\int_0^\infty \Psi(\xi)\mathrm{d}\xi = \pi \text{ and } \int_0^\infty \widehat{\rho_Y}(\xi)\mathrm{d}\xi = c^2\pi. \qquad \square$$

2.1. Simulation of the iGLE

We will actually be simulating the integral $Z(t)$ of solutions to the GLE $Y(t)$ as defined by (4). We summarize our algorithm here. From the preceding discussion, we know that $Y(t)$ is a Gaussian, stationary process with known covariance $\rho_Y(t-s)$ and that $Z(t)$ is a Gaussian, non-stationary process with covariance

$$\rho_Z(t,s) = \int_0^t \int_0^s \rho_Y(t'-s')\mathrm{d}t'\mathrm{d}s'$$

for $t > s$. Changing variables and reversing the order of integration, we rewrite $\rho_Z(t,s)$ in terms of moments of ρ_Y. Namely we have

$$\rho_Z(t,s) = tI_1(t) - (t-s)I_1(t-s) + sI_1(s) - [I_2(t) - I_2(t-s) + I_2(s)],$$

where $I_1(t) = \int_0^t \rho_Y(u)\mathrm{d}u$ and $I_2(t) = \int_0^t u\rho_Y(u)\mathrm{d}u$. Since, in general, we know ρ_Y through its Fourier transform, $\widehat{\rho_Y}$, we use the inverse Fourier transform and the fact that $\rho_Z(t,s)$ is real to express the integrals in a more manageable form. We find

$$\rho_Z(t,s) = J(t) + J(s) - J(t-s) \text{ where} \tag{11}$$

$$J(t) = \frac{2}{\pi}\int_0^\infty \frac{\widehat{\rho_Y}(\xi)}{\xi^2}\sin^2\left(\frac{\xi t}{2}\right)\mathrm{d}\xi. \tag{12}$$

We note that since the integrand can be analytically continued at $\xi = 0$ and $\widehat{\rho_Y}$ is integrable, the integral $J(t)$ is well defined.

The last step of the simulation is a covariance based algorithm to obtain realizations of the iGLE $Z(t)$. We define Z_i to be one realization of the path $Z(t_i) = \int_0^{t_i} Y(s)\mathrm{d}s$ with $t_i = i\Delta t$ and $i = 1, \cdots, N_T$ and $Z_0 = 0$. Further, we define the discrete covariance matrix $\mathbf{R}$ as $R_{ij} = \rho_Z(t_i, t_j)$ for $1 \le i, j \le N_T$. Following [39], the random variable $\mathbf{Z} = (Z_1, \ldots, Z_{N_T})^T$ given as

$$\mathbf{Z} = \mathbf{C}\mathbf{W} \quad \mathbf{W} \sim \mathcal{N}(0,1)^N, \tag{13}$$

where $\mathbf{W}$ is a vector of mean one normal variables and $\mathbf{C}$ is the lower triangular Cholesky factorization of $\mathbf{R}$, in other words $\mathbf{R} = \mathbf{C}\mathbf{C}^T$, has the correct statistical structure. Since $\mathbf{R}$ is a covariance matrix, it is symmetric, positive semi-definite and its Cholesky decomposition exists. Since the memory kernels $K(t)$ that we use are nonzero for all t, all entries of $\mathbf{R}$ are nonzero as well.

In summary, the algorithm to realize one path of the iGLE is

1. Build the discrete symmetric covariance matrix $R_{ij} = \rho_Z(t_i, t_j)$ for $1 \le i, j \le N_T$ using (11);
2. Find the lower triangular Cholesky decomposition $\mathbf{C}$ of $\mathbf{R}$;
3. Find a realization of the path $\mathbf{Z}$ with $Z_0 = 0$ using (13);
4. Calculate the increment $\Delta Z_i = Z_{i+1} - Z_i$ for $i = 1, \ldots, N_T$.

Further discussions of the accuracy of the integral calculation as it pertains to the iGLE stemming from the fluid model are discussed in Section 5.

3. Particle–fluid model

3.1. Viscoelastic fluid model in real space

A common method to derive tractable models of the effect of complex fluids on immersed particles is to coarse-grain molecular deterministic equations over an appropriate length scale. Here, we extend the work of [26,27,40] for a viscous fluid with thermal fluctuations to include viscoelastic stresses by first considering the incompressible Navier–Stokes equation for a fluid velocity field $\mathbf{u}$ without external forces

$$\rho(\partial_t\mathbf{u} + \mathbf{u}\cdot\nabla\mathbf{u}) = \nabla\cdot\mathbf{\Sigma}, \quad \nabla\cdot\mathbf{u} = 0, \tag{14}$$

where ρ is the fluid density and $\mathbf{\Sigma}$ is the total stress. We assume periodic boundary conditions with period of length $2\pi L$. The total stress tensor is comprised of two components: a deterministic viscoelastic stress $\mathbf{\Sigma}_{\mathrm{det}}$ and a stochastic stress $\mathbf{\Sigma}_{\mathrm{stoch}}$.

Following Larson [41], the deterministic stress tensor can be decomposed into a solvent contribution $\mathbf{\Sigma}_{\mathrm{det,s}}$ and a polymeric contribution $\mathbf{\Sigma}_{\mathrm{det,p}}$. The solvent stress is the Newtonian stress tensor

$$\mathbf{\Sigma}_{\mathrm{det,s}} = -p\mathbf{I} + 2\eta_s\mathbf{E}, \tag{15}$$

where p is the pressure, $\mathbf{I}$ is the identity matrix, $\mathbf{E} = (\nabla\mathbf{u} + \nabla\mathbf{u}^T)/2$ is the rate-of-strain tensor, and η_s is the solvent dynamic viscosity. As in [31,41–43], we consider the small strain limit for the polymeric stress tensor resulting in a linear viscoelastic model. In this setting, the constitutive equation for $\mathbf{\Sigma}_{\text{det,p}}$ is known as the Lodge equation and it has the form

$$\mathbf{\Sigma}_{\text{det,p}} = G_{\text{avg}}\mathbf{I} + 2\int_{-\infty}^{t} G_{(r)}(t-t')\mathbf{E}(t')\mathrm{d}t', \tag{16}$$

where G_{avg} is the mean stress and $G_{(r)}(t)$ is the relaxation modulus (units of [stress]). The response is causal in the sense that $G_{(r)}(t) = 0$ for $t < 0$. Combining (15) and (16), we have

$$\mathbf{\Sigma}_{\text{det}} = -(p - G_{\text{avg}})\mathbf{I} + 2\eta_s\mathbf{E} + 2\int_{-\infty}^{t} G_{(r)}(t-t')\mathbf{E}(t')\mathrm{d}t'. \tag{17}$$

The zero shear-rate viscosity η_0 is related to $G_{(r)}(t)$ by $\eta_0 = \eta_s + \int_0^\infty G_{(r)}(t')\mathrm{d}t'$.

If $G_{(r)}(t)$ is a single mode Maxwell model, $G_{(r)} = \frac{\eta_p}{\tau}e^{-t/\tau}$, where τ is the relaxation time and η_p is the polymeric dynamic viscosity related to G_{avg} by $\eta_p = G_{\text{avg}}\tau$ [41], then $\boldsymbol{\sigma}_{\text{set}} = \mathbf{\Sigma}_{\text{det}} + (p - G_{\text{avg}})\mathbf{I}$ satisfies the Oldroyd-B equation

$$\tau\overset{\triangledown}{\boldsymbol{\sigma}}_{\text{det}} + \boldsymbol{\sigma}_{\text{det}} = 2\eta_0\left(\mathbf{E} + \frac{\tau\eta_s}{\eta_0}\overset{\triangledown}{\mathbf{E}}\right),$$

where $\eta_0 = \eta_s + \eta_p$, and $\overset{\triangledown}{\cdot}$ is the upper convected time derivative defined as $\overset{\triangledown}{\mathbf{S}} = \frac{d\mathbf{S}}{dt} - \nabla\mathbf{u}^T\mathbf{S} - \mathbf{S}\nabla\mathbf{u}$. If the solvent viscosity is negligible, $\eta_s = 0$, then $\boldsymbol{\sigma}_{\text{det}}$ satisfies the Upper Convected Maxwell equation

$$\tau\overset{\triangledown}{\boldsymbol{\sigma}}_{\text{det}} + \boldsymbol{\sigma}_{\text{det}} = 2\eta_p\mathbf{E}.$$

In this paper, we use a generalized form of $G_{(r)}(t)$ known as the N-Maxwell model, a sum of N exponential terms

$$G_{(r)}(t) = \frac{1}{N}\sum_{n=0}^{N-1} G_n e^{-t/\tau_n} \text{ for } t \geq 0, \tag{18}$$

where τ_n are the relaxation times of the polymeric fluid component. By construction, the polymeric viscosity and mean stress are

$$\eta_p = \frac{1}{N}\sum_{n=0}^{N-1} G_n\tau_n \quad \text{and} \quad G_{\text{avg}} = \frac{1}{N}\sum_{n=0}^{N-1} G_n.$$

We pick equal size for all G_n, which we represent by G_0. In this case, $\eta_p = G_0\tau_{\text{avg}}$ and $G_{\text{avg}} = G_0$. To simplify notation later, we define a dimensionless relaxation kernel $K(t)$ so Eq. (18) becomes

$$G_{(r)}(t) = \begin{cases} \frac{\eta_p}{\tau_{\text{avg}}}K(t), & t \geq 0 \\ 0, & t < 0 \end{cases} \text{ with } K(t) = \frac{1}{N}\sum_{n=0}^{N-1} e^{-|t|/\tau_n} \text{ for all } t. \tag{19}$$

Altogether, substituting Eq. (19) into Eq. (17), we have

$$\mathbf{\Sigma}_{\text{det}} = -\left(p - \frac{\eta_p}{\tau_{\text{avg}}}\right)\mathbf{I} + 2\eta_s\mathbf{E} + 2\frac{\eta_p}{\tau_{\text{avg}}}\int_{-\infty}^{t} K(t-t')\mathbf{E}(t')\mathrm{d}t'. \tag{20}$$

There are random fluctuations in the stress tensor due to thermal energy. As with the deterministic contribution to the stress tensor, we separate $\mathbf{\Sigma}_{\text{stoch}}$ into two terms: $\mathbf{\Sigma}_{\text{stoch,s}}$ and $\mathbf{\Sigma}_{\text{stoch,p}}$. Following Pitaevskii & Lifschitz [40], the solvent fluctuation term has the form

$$\mathbf{\Sigma}_{\text{stoch,s}} = \sqrt{2k_BT\eta_s}\dot{\mathbf{W}} \tag{21}$$

where $\dot{\mathbf{W}}$ is a space–time white noise tensor, formally satisfying

$$\mathbb{E}\left[\dot{W}_{ij}(\mathbf{x},t)\dot{W}_{mn}(\mathbf{y},s)\right] = (\delta_{im}\delta_{jn} + \delta_{in}\delta_{jm})\delta(\mathbf{x}-\mathbf{y})\delta(t-s). \tag{22}$$

The first term in parenthesis on the right of (22) has the form

$$\delta_{im}\delta_{jn}+\delta_{in}\delta_{jm}=\begin{cases}1 & \text{if } m\neq n \;\&\; [(i=m \;\&\; j=n)||(i=n \;\&\; j=m)]\\ 2 & \text{if } i=j=m=n\\ 0 & \text{otherwise}\end{cases}.$$

This encodes the properties that distinct noise components are independent and the resulting stress tensor is isotropic, symmetric and traceless. The leading coefficient of (21) follows from a computation of the kinetic energy discussed in Section 3.5.

The polymer fluctuation stress term has the form

$$\boldsymbol{\Sigma}_{\text{stoch,p}}=\sqrt{k_BT\eta_p/\tau_{\text{avg}}}\mathbf{F}, \tag{23}$$

where $\mathbf{F}$ is a stationary, mean zero Gaussian noise process that is white in space, but not in time. In accordance with the fluctuation–dissipation relationship [40], the memory structure of the thermal fluctuations matches that of the deterministic part in the following way:

$$\mathbb{E}\left[F_{ij}(\mathbf{x},t)F_{mn}(\mathbf{y},s)\right]=(\delta_{im}\delta_{jn}+\delta_{in}\delta_{jm})\delta(\mathbf{x}-\mathbf{y})K(t-s) \tag{24}$$

where K is the memory kernel introduced in Eq. (19). We note the presence of a two in (21) but not in (23). This is again a consequence of equipartition of energy discussed in Section 3.5.

After collecting the deterministic and stochastic stress terms of (20), (21), and (23) and recalling that $2\nabla\cdot\mathbf{E}=\Delta\mathbf{u}$, our thermally fluctuating viscoelastic fluid model is described by the stochastic partial-integro-differential equation

$$\begin{aligned}\rho(\partial_t\mathbf{u}+\mathbf{u}\cdot\nabla\mathbf{u})=&-\nabla\left(p-\frac{\eta_p}{\tau_{\text{avg}}}\right)+\eta_s\Delta\mathbf{u}+\frac{\eta_p}{\tau_{\text{avg}}}(K^+*\Delta\mathbf{u})\\&+\sqrt{2k_BT\eta_s}\nabla\cdot\dot{\mathbf{W}}+\sqrt{k_BT\eta_p/\tau_{\text{avg}}}\nabla\cdot\mathbf{F}\end{aligned} \tag{25}$$

with the incompressibility condition $\nabla\cdot\mathbf{u}=0$. In the above, $K^+(t)=\mathbb{1}_{\{t\geq 0\}}(t)K(t)$ (with $\mathbb{1}$ being the indicator function), $*$ denotes convolution in time and the functions K, $\dot{\mathbf{W}}$ and $\mathbf{F}$ are defined by Eqs. (19), (22) and (24), respectively. For simplicity of notation, in the reminder of this paper, we rescale the pressure to just p instead of $p-\eta_p/\tau_{\text{avg}}$.

3.2. Definition of the noise

Throughout this work, we assume periodic boundary conditions for the fluid, for the moment defining the domain to be $\mathcal{O}=[0,2\pi L]^d$, where d is the number of dimensions. We define the associated Fourier transform pair of a periodic function $f(\mathbf{x})$ as

$$f(\mathbf{x})=\sum_{\mathbf{k}\in\mathbb{Z}^d}f_{\mathbf{k}}e^{i\mathbf{k}\cdot\mathbf{x}/L}\quad f_{\mathbf{k}}=\frac{1}{(2\pi L)^d}\int_{\mathcal{O}}f(\mathbf{x})e^{-i\mathbf{k}\cdot\mathbf{x}/L}\mathrm{d}\mathbf{x}.$$

Our definition for the stationary Gaussian noise $\mathbf{F}$ is then

$$\mathbf{F}(\mathbf{x},t):=\frac{1}{(2\pi L)^{d/2}}\sum_{\mathbf{k}\in\mathbb{Z}^d}\mathbf{F}^{\mathbf{k}}(t)e^{i\mathbf{k}\cdot\mathbf{x}/L},$$

where $\mathbf{F}^{\mathbf{k}}(t)$ is a collection of mean zero complex valued stationary processes satisfying

$$\mathbb{E}\left[F^{\mathbf{k}}_{ij}(t)\overline{F^{\mathbf{l}}_{mn}(s)}\right]=(\delta_{im}\delta_{jn}+\delta_{in}\delta_{jm})\delta_{\mathbf{kl}}K(t-s). \tag{26}$$

With the above definition, we have

$$\begin{aligned}\mathbb{E}\left[F_{ij}(\mathbf{x},t)F_{mn}(\mathbf{y},s)\right]&=\frac{1}{(2\pi L)^d}\sum_{\mathbf{k},\mathbf{l}}\mathbb{E}\left[F^{\mathbf{k}}_{ij}(t)\overline{F^{\mathbf{l}}_{mn}(s)}\right]e^{i\mathbf{k}\cdot\mathbf{x}/L}e^{-i\mathbf{l}\cdot\mathbf{y}/L}\\&=(\delta_{im}\delta_{jn}+\delta_{in}\delta_{jm})\frac{1}{(2\pi L)^d}\sum_{\mathbf{k}}e^{i\mathbf{k}\cdot(\mathbf{x}-\mathbf{y})/L}K(t-s)\\&=(\delta_{im}\delta_{jn}+\delta_{in}\delta_{jm})\delta(\mathbf{x}-\mathbf{y})K(t-s),\end{aligned}$$

which agrees with Eq. (24). In the above, we used

$$\delta(\mathbf{x}-\mathbf{y})=\frac{1}{(2\pi L)^d}\sum_{\mathbf{k}}e^{i\mathbf{k}\cdot(\mathbf{x}-\mathbf{y})/L}.$$

A similar definition and decomposition hold for $\dot{\mathbf{W}}$ with $K(t-s)$ being replaced by $\delta(t-s)$.

3.3. Non-dimensionalization

Dividing (25) by ρ and letting $\nu_s = \eta_s/\rho$ and $\nu_p = \eta_p/\rho$ be the kinematic viscosities, we have

$$\partial_t \mathbf{u} + \mathbf{u}\cdot\nabla\mathbf{u} = -\frac{1}{\rho}\nabla p + \nu_s\Delta\mathbf{u} + \frac{\nu_p}{\tau_{\text{avg}}}(K^+ * \Delta\mathbf{u}) + \sqrt{\frac{2k_BT\nu_s}{\rho}}\,\nabla\cdot\dot{\mathbf{W}} + \sqrt{\frac{k_BT\nu_p}{\rho\tau_{\text{avg}}}}\,\nabla\cdot\mathbf{F}. \tag{27}$$

In order to non-dimensionalize this system, it is worth first recalling the method used for models of individual particle motion with velocity processes that are given by the Langevin Equation and the GLE. For the first case, consider the SDE

$$\mathrm{d}Y(t) = -aY(t)\mathrm{d}t + c\sqrt{2a}\mathrm{d}W(t),\ Y(0) = y, \tag{28}$$

where the initial value y is drawn from the stationary distribution, $y \sim N(0, c^2)$. In physical terms, $a = \gamma_s/m$ (units of $[\texttt{time}^{-1}]$) and $c = \sqrt{k_BT/m}$ (units of $[\texttt{length/time}]$). Formally, it is customary to consider the noise $\mathrm{d}W(t)$ to have units of $[\texttt{time}^{-1/2}]$, but it is perhaps more transparent to understand how the units work out by looking at the second moment of $Y(t)$.

By Itô's Formula,

$$\mathrm{d}Y^2(t) = -2aY^2(t) + c^2a\mathrm{d}t + 2aY(t)\mathrm{d}W(t).$$

Taking expectation on both sides and solving this resulting ODE yields [44]

$$\mathbb{E}\left[Y^2(t)\right] = c^2 + \left(\mathbb{E}\left[y^2\right] - c^2\right)e^{-2at}.$$

Under the assumption that $y \sim N(0, c^2)$ we see that $\mathbb{E}\left[Y^2(t)\right] = c^2$, meaning that c must have the same units as Y.

Moving on to the nondimensionalization, the coefficient a sets the time scale of the system, so we define the non-dimensional time to be $\tilde{t} = at$. Meanwhile, we use the standard deviation of the stationary distribution to rescale $Y(t)$. As such, we define $c\tilde{Y}(\tilde{t}) := Y(t)$. Then, using the integral form of (28), we have

$$\tilde{Y}(\tilde{t}) - \tilde{Y}(0) = \frac{1}{c}\left(Y(t) - y\right) = \frac{1}{c}\Big(-\int_0^t aY(s)ds + c\sqrt{2a}W(t)\Big).$$

For the integral, we adopt the substitution $u = as$ and for the Brownian motion term, we observe the rescaling law, $\sqrt{a}W(t) \sim W(at)$. Then

$$\tilde{Y}(\tilde{t}) - \tilde{Y}(0) = -\frac{1}{c}\int_0^{at} Y\Big(\frac{u}{a}\Big)du + \sqrt{2}\,W(at) = -\int_0^{\tilde{t}} \tilde{Y}(u)\mathrm{d}u + \sqrt{2}\,W(\tilde{t}),$$

which is to say that $\tilde{Y}$ satisfies the integral form of the Langevin Equation with a stationary distribution that has mean zero and variance one.

We now extend this to the GLE (4), which has the integral form

$$Y(t) - y = -a\int_0^t Y(s)\mathrm{d}s - b\int_0^t\int_{-\infty}^{t'} K(t'-s')Y(s')\mathrm{d}s'\mathrm{d}t' + c\sqrt{2a}W(t) + c\sqrt{b}F(t). \tag{29}$$

As before, we use the time-scale $\tilde{t} = at$, and then define $\tilde{K}(\tilde{t}) := K(t)$ and $\tilde{F}(\tilde{t}) := F(t)$. In this way,

$$\mathbb{E}\left[\tilde{F}(\tilde{t})\tilde{F}(\tilde{s})\right] = \mathbb{E}\left[F(t)F(s)\right] = K(t-s) = \tilde{K}(\tilde{t}-\tilde{s}).$$

Again let $c\tilde{Y}(\tilde{t}) := Y(t)$. Multiplying the right-hand side of (29) by $1/c$ and adopting the substitutions $\tilde{t}' = at'$ and $\tilde{s}' = as'$, we have for the double integral term

$$\frac{b}{c}\int_0^t\int_{-\infty}^{t'} K(t'-s')Y(s')\mathrm{d}t'\mathrm{d}s' = \frac{b}{a^2}\int_0^{\tilde{t}}\int_{-\infty}^{\tilde{t}'} \tilde{K}(\tilde{t}'-\tilde{s}')\tilde{Y}(\tilde{s}')\mathrm{d}\tilde{s}'\mathrm{d}\tilde{t}'.$$

Together with the other terms, the non-dimensional (differential) version of the GLE is given by

$$\mathrm{d}\tilde{Y}(\tilde{t}) = \Big(-\tilde{Y}(\tilde{t}) - \beta\int_{-\infty}^{\tilde{t}} \tilde{K}(\tilde{t}-\tilde{s})\tilde{Y}(\tilde{s})\mathrm{d}\tilde{s} + \sqrt{\beta}\tilde{F}(\tilde{t})\Big)\mathrm{d}t + \sqrt{2}\,\mathrm{d}W(\tilde{t}), \tag{30}$$

where $\beta = b/a^2$.

To generalize these observations to the stochastic Navier–Stokes equations, we set the following nondimensional quantities:

$$\mathbf{u} = U\tilde{\mathbf{u}} \quad \mathbf{x} = L\tilde{\mathbf{x}} \quad t = \theta\tilde{t}.$$

Noting that the kinematic viscosity has units of $[\mathtt{length}^2/\mathtt{time}]$, it is natural to use the dissipative time scale $\theta = L^2/\nu_s$. This definition is consistent with our treatment of the time scale $a^{-1} = m/\gamma_s$ in the GLE, recalling that $1/\nu_s = \rho/\eta_s$ and that $\gamma_s = 6\pi a\eta_s$. The appearance of the L^2 is due to the two spatial derivatives in the Laplacian. For U, we have the definition $U = \sqrt{k_B T/\rho L^d}$. The term $k_B T/m$ from the GLE is replaced by $k_B T/\rho$ and the choice for the power of L becomes clear after we appropriately rescale the noise terms. To this end, we introduce (with appropriately redefined tildes)

$$\tilde{\mathbf{F}}(\tilde{\mathbf{x}},\tilde{t}) := \frac{1}{(2\pi)^{d/2}}\sum_{\mathbf{k}}\tilde{\mathbf{F}}^{\mathbf{k}}(\tilde{t})e^{i\mathbf{k}\cdot\tilde{\mathbf{x}}} = \frac{L^{d/2}}{(2\pi L)^{d/2}}\sum_{\mathbf{k}}\mathbf{F}^{\mathbf{k}}(t)e^{i\mathbf{k}\cdot\mathbf{x}/L} = L^{d/2}\mathbf{F}(\mathbf{x},t), \tag{31}$$

where for each $\mathbf{k}$, $\tilde{\mathbf{F}}^{\mathbf{k}}(\tilde{t}) = \mathbf{F}^{\mathbf{k}}(t)$. Meanwhile,

$$\begin{aligned}\tilde{\mathbf{W}}(\tilde{\mathbf{x}},\tilde{t}) :=& \frac{1}{(2\pi)^{d/2}}\sum_{\mathbf{k}}\mathbf{W}^{\mathbf{k}}(\tilde{t})e^{i\mathbf{k}\cdot\tilde{\mathbf{x}}}\\ =& \frac{L^{d/2}}{(2\pi L)^{d/2}}\sum_{\mathbf{k}}\frac{1}{\sqrt{\theta}}\mathbf{W}^{\mathbf{k}}(t)e^{i\mathbf{k}\cdot\mathbf{x}/L} = \frac{L^{d/2}}{\sqrt{\theta}}\mathbf{W}(\mathbf{x},t).\end{aligned} \tag{32}$$

Throughout this paper, we will consider finite dimensional truncations for the sum over $\mathbf{k}$. It follows from (31) and (32) that both $\mathbf{F}$ and $\mathbf{W}$ are smooth in $\mathbf{x}$, so there is no issue in discussing the divergence of these random fields. We then see that

$$\tilde{\nabla}\cdot\tilde{\mathbf{F}}(\tilde{x},\tilde{t}) = L^{(d+2)/2}\,\nabla\cdot\mathbf{F}(x,t);\ \text{and,}$$
$$\tilde{\nabla}\cdot\tilde{\mathbf{W}}(\tilde{x},\tilde{t}) = \theta^{-\frac{1}{2}}L^{(d+2)/2}\,\nabla\cdot\mathbf{W}(x,t).$$

As is common in flow in which viscous force dominates, we set $p = P\tilde{p}$ with $P = \rho LU/\theta$ for the non-dimensional pressure. Substituting these definitions in Eq. (27), we find

$$\partial_{\tilde{t}}\tilde{\mathbf{u}} + \mathrm{Re}\,\tilde{\mathbf{u}}\cdot\tilde{\nabla}\tilde{\mathbf{u}} = -\tilde{\nabla}\tilde{p} + \tilde{\Delta}\tilde{\mathbf{u}} + \beta(\tilde{K}^+ * \tilde{\Delta}\tilde{\mathbf{u}}) + \sqrt{2}\tilde{\nabla}\cdot\dot{\mathbf{W}} + \sqrt{\beta}\tilde{\nabla}\cdot\tilde{\mathbf{F}},$$

where $\mathrm{Re} = UL/\nu_s$ is the Reynolds number and

$$\beta := \frac{\nu_p L^2}{\nu_s^2\tau_{\mathrm{avg}}} = \frac{G_0\rho L^2}{\eta_s^2}$$

is a new dimensionless group. For low Reynolds number, we neglect the nonlinear term, and dropping the tildes, the above equation reduces to

$$\partial_t\mathbf{u} = -\nabla p + \Delta\mathbf{u} + \beta(K^+ * \Delta\mathbf{u}) + \sqrt{2}\nabla\cdot\dot{\mathbf{W}} + \sqrt{\beta}\nabla\cdot\mathbf{F}, \tag{33}$$

which is a natural form, given the non-dimensional GLE (30).

3.4. Transformation to Fourier space

Henceforth we consider the two-dimensional version of (33), periodic with domain $\mathcal{O} = [0, 2\pi]^2$. We now proceed as in the non-fluctuating case and transform (33) together with $\nabla\cdot\mathbf{u} = 0$ into Fourier space. To do so, we express $\mathbf{u}(\mathbf{x},t)$ and $p(\mathbf{x},t)$ through their Fourier series:

$$\mathbf{u}(\mathbf{x},t) = \sum_{\mathbf{k}\in\mathcal{K}}\mathbf{u}_{\mathbf{k}}(t)e^{i\mathbf{k}\cdot\mathbf{x}} \quad p(\mathbf{x},t) = \sum_{\mathbf{k}\in\mathcal{K}}p_k(t)e^{i\mathbf{k}\cdot\mathbf{x}}$$

where $\mathcal{K} = \mathbb{Z}^2\setminus\mathbf{0}$. Because our system is assumed to have mean zero velocity, $\mathbf{u_0}(t) = 0$ for all t. Also note that the Fourier transformed version of the incompressibility condition is that $\mathbf{k}^T\mathbf{u}_{\mathbf{k}} = 0$ for all $\mathbf{k}$.

Before eliminating the pressure, we remark that the divergence of a tensor in Fourier space can be written as

$$\begin{aligned}\nabla\cdot\mathbf{F} = \partial_m F_{mj}\mathbf{e}_j &= \frac{1}{2\pi}\sum_{\mathbf{k}\in\mathbb{Z}^2}\partial_m e^{i\mathbf{k}\cdot\mathbf{x}}F^{\mathbf{k}}_{mj}(t)\mathbf{e}_j = \frac{i}{2\pi}\sum_{\mathbf{k}\in\mathbb{Z}^2}k_m F^{\mathbf{k}}_{mj}(t)\mathbf{e}_j e^{i\mathbf{k}\cdot\mathbf{x}}\\ &\overset{\mathbf{F}\,\mathrm{sym}}{=} \frac{i}{2\pi}\sum_{\mathbf{k}\in\mathbb{Z}^2}F^{\mathbf{k}}_{jm}(t)k_m\mathbf{e}_j e^{i\mathbf{k}\cdot\mathbf{x}} = \frac{i}{2\pi}\sum_{\mathbf{k}\in\mathbb{Z}^2}e^{i\mathbf{k}\cdot\mathbf{x}}\mathbf{F}^{\mathbf{k}}(t)\mathbf{k}.\end{aligned}$$

In the above, $\overset{\mathbf{F}\,\mathrm{sym}}{=}$ denotes the use of the symmetry relation $F^{\mathbf{k}}_{mj}(t) = F^{\mathbf{k}}_{jm}(t)$. A similar formulation holds for the divergence of $\mathbf{W}$.

Defining $\hat{\mathbf{k}} = \frac{1}{k}\mathbf{k}$, where $k = |\mathbf{k}|$, taking the dot product of the Fourier transform of (33) with $\hat{\mathbf{k}}$, and using $\mathbf{k}^T\mathbf{u}_{\mathbf{k}} = 0$, we find

$$p_k = \frac{1}{2\pi}\left(\sqrt{2}\hat{\mathbf{k}}^T\dot{\mathbf{W}}^{\mathbf{k}}\hat{\mathbf{k}} + \sqrt{\beta}\hat{\mathbf{k}}^T\mathbf{F}^{\mathbf{k}}\hat{\mathbf{k}}\right). \tag{34}$$

Plugging (34) back into the Fourier transform of (33), we obtain

$$\partial_t\mathbf{u}_{\mathbf{k}} = -k^2\mathbf{u}_{\mathbf{k}} - \beta k^2(K^+ * \mathbf{u}_{\mathbf{k}}) + \frac{i\sqrt{2}}{2\pi}\mathbf{P}^{\mathbf{k}}\dot{\mathbf{W}}^{\mathbf{k}}\mathbf{k} + \frac{i\sqrt{\beta}}{2\pi}\mathbf{P}^{\mathbf{k}}\mathbf{F}^{\mathbf{k}}\mathbf{k}. \tag{35}$$

Here $\mathbf{P}$ is the projection matrix onto the space of incompressible solutions given as $\mathbf{P}^{\mathbf{k}} = \mathbf{I} - \hat{\mathbf{k}}\hat{\mathbf{k}}^T$.

Because the initial condition is real, $\mathbf{u}$ is real and thus $\mathbf{u}_{-\mathbf{k}} = \overline{\mathbf{u}_{\mathbf{k}}}$. Therefore, we will work with the corresponding real and imaginary parts of the complex equation (35). Let $\mathbf{v}_{\mathbf{k}} = \mathrm{Re}(\mathbf{u}_{\mathbf{k}})$ and $\mathbf{w}_{\mathbf{k}} = \mathrm{Im}(\mathbf{u}_{\mathbf{k}})$ be the real and imaginary parts of $\mathbf{u}_{\mathbf{k}}$ respectively. Since $\mathbf{F}^{\mathbf{k}}$ is a complex stochastic process, it can be written as $\mathbf{F}^{\mathrm{real},\mathbf{k}} + i\mathbf{F}^{\mathrm{im},\mathbf{k}}$, so that $\mathbb{E}\left[F^{\mathrm{real},\mathbf{k}}_{ij}(t)F^{\mathrm{real},\mathbf{l}}_{mn}(s)\right] = \mathbb{E}\left[F^{\mathrm{im},\mathbf{k}}_{ij}(t)F^{\mathrm{im},\mathbf{l}}_{mn}(s)\right] = \frac{1}{2}\mathbb{E}\left[F^{\mathbf{k}}_{ij}(t)F^{\mathbf{l}}_{mn}(s)\right]$, and similarly for $\dot{\mathbf{W}}^{\mathbf{k}}$. Taking the complex conjugate of (35) adding it to itself, and dividing by 2, we have

$$\partial_t\mathbf{v}_{\mathbf{k}} = -k^2\mathbf{v}_{\mathbf{k}} - \beta k^2(K^+ * \mathbf{v}_{\mathbf{k}}) + \frac{\sqrt{2}k}{2\pi}\mathbf{P}^{\mathbf{k}}\dot{\mathbf{W}}^{\mathrm{im},\mathbf{k}}\hat{\mathbf{k}} + \frac{\sqrt{\beta}k}{2\pi}\mathbf{P}^{\mathbf{k}}\mathbf{F}^{\mathrm{im},\mathbf{k}}\hat{\mathbf{k}} \tag{36}$$

and similarly for $\mathbf{w}_{\mathbf{k}}$ with noise $\mathbf{F}^{\mathrm{real},\mathbf{k}}$ and $\dot{\mathbf{W}}^{\mathrm{real},\mathbf{k}}$.

Equation (36) is a vector equation, which we can decompose in terms of its components. To do so, we let $\mathbf{v}_{\mathbf{k}} = \mathbf{P}^{\mathbf{k}}\boldsymbol{\zeta}^{\mathbf{k}}\hat{\mathbf{k}}$, where $\boldsymbol{\zeta}$ is a 2×2 matrix, and plug into (36). We obtain for the components of $\boldsymbol{\zeta}$

$$\begin{aligned}
\partial_t\zeta^{\mathbf{k}}_{ij} &= -k^2\zeta^{\mathbf{k}}_{ij} - \beta k^2(K^+ * \zeta^{\mathbf{k}}_{ij}) + \frac{\sqrt{2}k}{2\pi}\dot{W}^{\mathrm{im},\mathbf{k}}_{ij} + \frac{\sqrt{\beta}k}{2\pi}F^{\mathrm{im},\mathbf{k}}_{ij} \\
\mathbb{E}\left[F^{\mathrm{im},\mathbf{k}}_{ij}(t)F^{\mathrm{im},\mathbf{l}}_{mn}(s)\right] &= K(t-s)\frac{1}{2}\left(\delta_{im}\delta_{jn} + \delta_{in}\delta_{jm}\right) \\
\mathbb{E}\left[\dot{W}^{\mathrm{im},\mathbf{k}}_{ij}(t)\dot{W}^{\mathrm{im},\mathbf{l}}_{mn}(s)\right] &= \delta(t-s)\frac{1}{2}\left(\delta_{im}\delta_{jn} + \delta_{in}\delta_{jm}\right)
\end{aligned} \tag{37}$$

for all $\mathbf{k}, \mathbf{l}$ and $i, j, m, n = 1, 2$. Equation (37) is a GLE for each Fourier mode $\mathbf{k}$. Similarly, letting $\mathbf{w}_{\mathbf{k}} = \mathbf{P}^{\mathbf{k}}\boldsymbol{\xi}^{\mathbf{k}}\hat{\mathbf{k}}$, shows that $\mathbf{w}_{\mathbf{k}}$ is driven by a GLE for each Fourier mode.

3.5. Equipartition of energy

We now show that the fluctuating fluid system described by its Fourier modes in Section 3.4 satisfies equipartition of energy. By way of Parseval's Lemma, for all $t \in \mathbb{R}$,

$$\frac{1}{4\pi^2}\int_{\mathcal{O}} |\mathbf{u}(\mathbf{x}, t)|^2 d\mathbf{x} = \sum_{\mathbf{k}\in\mathcal{K}} |\mathbf{u}_{\mathbf{k}}(t)|^2. \tag{38}$$

Assuming that $\mathbf{u}(\mathbf{x}, t)$ is a stationary solution to (33), we can express the mean kinetic energy of the system in terms of the Fourier modes as follows:

$$\begin{aligned}
\mathscr{E} &= \frac{\rho}{2}\mathbb{E}\left[\int_{\mathcal{O}} |\mathbf{u}(\mathbf{x}, 0)|^2 d\mathbf{x}\right] = 2\pi^2\rho\sum_{\mathbf{k}\in\mathcal{K}}\mathbb{E}\left[|\mathbf{u}_{\mathbf{k}}(0)|^2\right] \\
&= 2\pi^2\rho\sum_{\mathbf{k}\in\mathcal{K}}(\mathbb{E}\left[|\mathbf{v}_{\mathbf{k}}|^2\right] + \mathbb{E}\left[|\mathbf{w}_{\mathbf{k}}|^2\right]) \\
&= 4\pi^2\rho\sum_{\mathbf{k}\in\mathcal{K}}\mathbb{E}\left[|\mathbf{v}_k|^2\right] \overset{\boldsymbol{\zeta}\,\mathrm{sym}}{=} 4\pi^2\rho\sum_{\mathbf{k}\in\mathcal{K}}\hat{\mathbf{k}}^T\mathbb{E}\left[\boldsymbol{\zeta}^{\mathbf{k}}\mathbf{P}^{\mathbf{k}}\boldsymbol{\zeta}^{\mathbf{k}}\right]\hat{\mathbf{k}},
\end{aligned} \tag{39}$$

where we dropped the dependence on the time $t = 0$ after the first line. From the $\delta_{im}\delta_{jn} + \delta_{in}\delta_{jm}$ term in the covariance structure of $\boldsymbol{\zeta}$ in Eq. (37), we know that the only non-zero terms in $\mathbb{E}\left[\boldsymbol{\zeta}^{\mathbf{k}}\mathbf{P}^{\mathbf{k}}\boldsymbol{\zeta}^{\mathbf{k}}\right]$ are

$$\mathbb{E}\left[(\zeta^{\mathbf{k}}_{11})^2\right], \mathbb{E}\left[(\zeta^{\mathbf{k}}_{12})^2\right] = \frac{1}{2}\mathbb{E}\left[(\zeta^{\mathbf{k}}_{11})^2\right], \mathbb{E}\left[(\zeta^{\mathbf{k}}_{22})^2\right] = \mathbb{E}\left[(\zeta^{\mathbf{k}}_{11})^2\right].$$

From the discussion about the generic GLE in Section 2 with $a = k^2, b = \beta k^2, c = \frac{1}{2\pi}$ and in particular Proposition 2.1, we have

$$\mathbb{E}\left[(\zeta_{11}^{\mathbf{k}})^2\right] = c^2 = \frac{1}{4\pi^2}.$$

Using the above results and carrying out the matrix multiplications, we find

$$\mathbb{E}\left[\boldsymbol{\zeta}^{\mathbf{k}}\mathbf{P}\boldsymbol{\zeta}^{\mathbf{k}}\right] = \frac{\mathbb{E}\left[(\zeta_{11})^2\right]}{2}\left(\hat{\mathbf{k}}^{\perp}\hat{\mathbf{k}}^{\perp^T} + \mathbf{I}\right) = \frac{1}{8\pi^2}\left(\hat{\mathbf{k}}^{\perp}\hat{\mathbf{k}}^{\perp^T} + \mathbf{I}\right),$$

where $\hat{\mathbf{k}}^{\perp} = (-k_2\, k_1)^T$ is the unit vector perpendicular to $\hat{\mathbf{k}} = (k_1\, k_2)^T$. Therefore, plugging back into (39), we find

$$\mathscr{E} = \frac{\rho}{2}\sum_{\mathbf{k}\in\mathcal{K}}\hat{\mathbf{k}}^T\left(\hat{\mathbf{k}}^{\perp}\hat{\mathbf{k}}^{\perp^T} + \mathbf{I}\right)\hat{\mathbf{k}} = \frac{\rho}{2}|\mathcal{K}|. \tag{40}$$

Thus each $\mathbf{u}_{\mathbf{k}}$ contributes the same amount to the kinetic energy. This result agrees with the equipartition theorem, which states, that because the fluid velocity can be written as a linear superposition of the Fourier modes $\{\mathbf{u}_k\}$, each mode should give an equal contribution to the kinetic energy [26].

3.6. Particle advection

We denote by $\mathbf{X}(t)$ the position of a particle and define the velocity of the particle as a distributional weighted average of the local fluid velocities

$$\frac{d\mathbf{X}(t)}{dt} = \mathbf{V}(t) = \int_{\mathbb{R}^d}\delta_a(\mathbf{x} - \mathbf{X}(t))\mathbf{u}(\mathbf{x}, t)d\mathbf{x}. \tag{41}$$

Here $\delta_a(\mathbf{x} - \mathbf{X}(t))$ is a smoothed delta function with length scale a, which is a proxy for particle radius. While there are many choices for δ_a [26], here we choose a Gaussian density function $\delta_a(\mathbf{y}) = (2\pi a^2)^{-d/2}\exp(-|\mathbf{y}|^2/(2a^2))$. Note that this function satisfies the scaling relation

$$L^d\delta_a(L\mathbf{x}) = \delta_{\frac{a}{L}}(\mathbf{x}).$$

While $\mathbf{u}$ is assumed to be periodic, $\mathbf{X}$ is not. Equation (41) is dimensional, so we non-dimensionalize it with the same scales as the fluid equations and introduce $\tilde{a} = a/L$. We find

$$\frac{d\tilde{\mathbf{X}}}{d\tilde{t}} = \frac{\theta U}{L}\int_{\mathbb{R}^d}\delta_{\tilde{a}}(\tilde{\mathbf{x}} - \tilde{\mathbf{X}}(\tilde{t}))\tilde{\mathbf{u}}(\tilde{\mathbf{x}}, \tilde{t})d\tilde{\mathbf{x}}.$$

Taking the specific case $d = 2$, we let $\tilde{\kappa}$ be the dimensionless pre-factor and drop the tilde notation to obtain

$$\frac{d\mathbf{X}(t)}{dt} = \mathbf{V}(t) = \kappa\int_{\mathbb{R}^2}\delta_a(\mathbf{x} - \mathbf{X}(t))\mathbf{u}(\mathbf{x}, t)d\mathbf{x}, \quad \kappa = \frac{\sqrt{k_B T\rho}}{\eta_s}. \tag{42}$$

The right-hand side of Eq. (42) is a convolution and can be expressed as a Fourier series

$$\mathbf{V}(t) = \kappa\sum_{\mathbf{k}\in\mathcal{K}}e^{i\mathbf{k}\cdot\mathbf{X}(t)}e^{-\frac{k^2a^2}{2}}\mathbf{u}_{\mathbf{k}}(t),$$

where we used the convolution theorem $(f * g)_{\mathbf{k}}(\mathbf{k}) = 4\pi^2 f_{\mathbf{k}}g_{\mathbf{k}}$ and the Fourier series of a Gaussian

$$\phi_{a,\mathbf{k}} = \frac{a^2}{2\pi}e^{-\frac{k^2a^2}{2}}.$$

Since $\mathbf{u}$ is real and thus $\mathbf{u}_{\mathbf{k}} = \overline{\mathbf{u}_{-\mathbf{k}}}$, we express the sum over $\mathcal{K}$ as twice the sum over $\mathcal{K}^+$, where $\mathcal{K}^+$ is the subset of $\mathcal{K}$ with $\mathbf{k} > 0$ in the product order. Decomposing into real and imaginary parts, we find

$$\frac{d\mathbf{X}}{dt} = \mathbf{V}(t) = 2\kappa\sum_{\mathbf{k}\in\mathcal{K}^+}\left[\cos(\mathbf{k}\cdot\mathbf{X}(t))\mathbf{v}_{\mathbf{k}}(t) - \sin(\mathbf{k}\cdot\mathbf{X}(t))\mathbf{w}_{\mathbf{k}}(t)\right]e^{-\frac{k^2a^2}{2}}. \tag{43}$$

4. Fluid–particle numerical methods

Because we are interested in particle updates, we discretize the particle position equation (44), but we never explicitly solve for the stochastic velocity fields $\mathbf{v_k}, \mathbf{w_k}$. The exact solution to the vector ODE (43) on an interval $[t, t+\Delta t]$ is

$$\mathbf{X}(t+\Delta t) - \mathbf{X}(t) = 2\kappa \sum_{\mathbf{k}\in\mathcal{K}^+} \int_t^{t+\Delta t} \Big[\cos(\mathbf{k}\cdot\mathbf{X}(s))\mathbf{v_k}(s) - \sin(\mathbf{k}\cdot\mathbf{X}(s))\mathbf{w_k}(s)\Big] ds\, e^{-\frac{k^2a^2}{2}}. \tag{44}$$

We discretize (44) with a semi-implicit Euler method. Using an explicit method like forward Euler would result in the wrong statistics at the end of the time interval as discussed in [26,45]. We denote by $\mathbf{X}_i$ the numerical approximation of $\mathbf{X}(t_i)$ where $t_i = i\Delta t$ and we consider N_T time steps, $i = 1, \dots, N_T$, starting with $\mathbf{X}_0 = (0.5\ 0.5)^T$. Using the decomposition of both $\mathbf{v_k}$ and $\mathbf{w_k}$ in terms of stochastic processes $\boldsymbol{\zeta}^{\mathbf{k}}$ and $\boldsymbol{\xi}^{\mathbf{k}}$ as derived in Section 3.4 and (44), the semi-implicit discretized particle update is then

$$X_{i+1,l} = X_{i,l} + 2\kappa \sum_{\mathbf{k}\in\mathcal{K}^+} P^{\mathbf{k}}_{lm} \Big[\cos(\mathbf{k}\cdot\mathbf{X}_i) \int_{t_i}^{t_{i+1}} \zeta^{\mathbf{k}}_{mn}(s) ds - \sin(\mathbf{k}\cdot\mathbf{X}_i) \int_{t_i}^{t_{i+1}} \xi^{\mathbf{k}}_{mn}(s) ds\Big] \frac{k_n}{k} e^{-\frac{k^2a^2}{2}}. \tag{45}$$

Here we adopted the Euler summation convention of repeated indices being summed over $\{1, 2\}$. For simplicity of exposure, we introduce the following notations

$$\int_0^{t_i} \zeta^{\mathbf{k}}_{mn}(s) ds = Z^{\mathbf{k}}_{i,mn}, \quad \int_0^{t_i} \xi^{\mathbf{k}}_{mn}(s) ds = \Xi^{\mathbf{k}}_{i,mn}$$

$$\Delta Z^{\mathbf{k}}_{i,mn} = Z^{\mathbf{k}}_{i+1,mn} - Z^{\mathbf{k}}_{i,mn}, \quad \Delta \Xi^{\mathbf{k}}_{i,mn} = \Xi^{\mathbf{k}}_{i+1,mn} - \Xi^{\mathbf{k}}_{i,mn}$$

and let $\mathcal{K}^+_M$ be the truncated set of the first M positive wave vectors. With these notations and (45), the numerical approximation of the particle update becomes

$$X_{i+1,l} = X_{i,l} + 2\kappa \sum_{\mathbf{k}\in\mathcal{K}^+_M} P^{\mathbf{k}}_{lm} \Big[\cos(\mathbf{k}\cdot\mathbf{X}_i)\Delta Z^{\mathbf{k}}_{i,mn} - \sin(\mathbf{k}\cdot\mathbf{X}_i)\Delta \Xi^{\mathbf{k}}_{i,mn}\Big] \frac{k_n}{k} e^{-\frac{k^2a^2}{2}}, \tag{46}$$

for $i = 0, \dots, N_T - 1$ with $\mathbf{X}_0 = (0.5\ 0.5)^T$ and $l = 1, 2$. To update the particle position with (46) we only need realizations of the integral increments $\Delta\mathbf{Z}^{\mathbf{k}}_i$ and $\Delta\boldsymbol{\Xi}^{\mathbf{k}}_i$ for $i = 0, \dots, N_T - 1$ where the underlying processes $\boldsymbol{\zeta}^{\mathbf{k}}$ and $\boldsymbol{\xi}^{\mathbf{k}}$ satisfy the GLEs (37) with appropriate covariance structure. The simulation of these increments was described in Section 2.1 for a generic GLE.

4.1. Numerical approximation of the integral $J(t)$

Before moving on, we note a difficulty that arises in the numerical integration of $J(t)$ given by Eq. (12) in the context of simulating the fluid Fourier modes. In the notation of Section 2, we have for the diagonal component of ζ_{ij} from (37) that $a = k^2$, $b = \beta k^2$, $c = \frac{1}{2\pi}$ with $k = |\mathbf{k}|$ and $\widehat{\rho_Y}(\xi)$ given by Eq. (7).

Since the tail of $\Psi(\xi)$ decays like ξ^{-2} and since $\Psi(0)$ and $\frac{\sin^2(\xi t/2)}{\xi^2}$ are well-defined at 0, the improper integral $J(t) = \frac{2c^2}{\pi k^2}\int_0^\infty \frac{\Psi(\xi)}{\xi^2}\sin\left(\frac{\xi t}{2}\right) d\xi$ exists. However, as illustrated in Fig. 1, the number of oscillations grows sharply as t increases. The number of oscillations renders the use of an adaptive scheme like Gauss–Kronod useless, as the number of sub-intervals needed to guarantee accuracy becomes unmanageable. Based on the proof of Proposition 2.1 and the subsequent residue formulas developed in [38], a residue method, where the pole of the numerators are known, would guarantee an exact evaluation of the integral. However, as N increases, the degree of the numerator of $\Psi(\xi)$ increases and computing the zeroes with any accuracy becomes impossible. Finally, if the Fourier inverse of $\widehat{\rho_Y}$ were known, then an FFT based method could be developed to evaluate $J(t)$. Such a method fails for N large due to the increasing length of the plateau and the slow onset of the decay of $\Psi(\xi)$ as seen in Fig. 4(b). Based on the above considerations, we numerically evaluate $J(t)$ using a trapezoidal rule on a non-equally spaced grid. Because $\sin^2(\xi t/2)/\xi^2$ is close to a sinc function, we use the `sincfun` package [46], which is a modification of the `chebfun` package [47] to properly handle integral of sinc type on a semi-infinite interval. Therefore, we let `sincfun` pick the location of the node to represent $\sin^2(\xi t/2)/\xi^2$ using sinc functions and use a trapezoidal rule with $\Psi(\xi)$ evaluated at the corresponding nodes. We note that the sinc objects can be pre-computed for every value of t and that only $\Psi(\xi)$ depends on k.

Any numerical errors in the evaluation of $J(t)$ will propagate into the positive semi-definite discrete covariance matrix $\mathbf{R}$ and might result in some of the smallest eigenvalues being negative. In order to still be able to compute the lower Cholesky decomposition of $\mathbf{R}$ we replace any small negative eigenvalues by a small positive tolerance. In practice, we observe that as t increases, the largest negative values range from 1×10^{-4} to 1×10^{-7}.

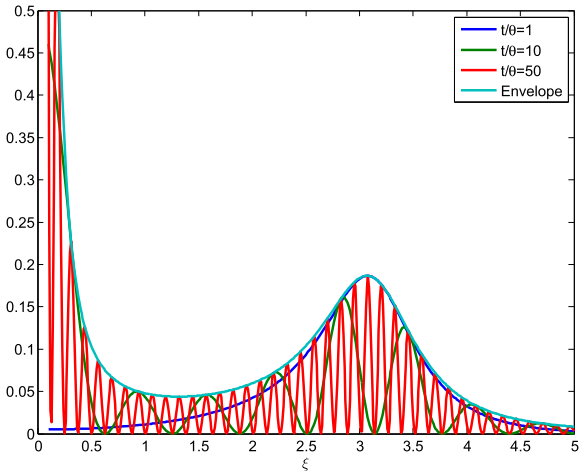

Fig. 1. Plot of $\Psi(\xi)\sin^2(\xi t/2)/\xi^2$, the integrand of $J(t)$, for $N=1$, $k=1$ at $t=10$ ms, 100 ms and 500 ms. The envelope (cyan) is given by $\Psi(\xi)/\xi^2$.

4.2. Computational costs

The computational cost of the two-step algorithm presented above is dominated by building the covariance matrix for each Fourier pair $\mathbf{k}$ and reading these matrices when updating the position of a particle. Once the physical parameters are fixed (including N_T), the covariance matrix for each of the Fourier mode GLE can be precomputed and stored. Since the GLE only depends on $|\mathbf{k}|$ only about $M/2$ matrices need to be saved. Using `sincfun`, most of the computational time in evaluating $J(t)$ is spent on building the sinc interpolant as opposed to evaluating the integral. We finally note that as N_T increases so does the computational cost of performing the Cholesky decomposition of each $N_T \times N_T$ matrix. The time to generate all the covariance matrices on a desktop for $M=256$ and $T_{\text{final}}=1024$ ms is about ten minutes. In comparison, the time to generate one corresponding particle path following Eq. (46) is about 1.6 s.

5. Behavior of the model and numerical results

5.1. Existence and uniqueness of the particle process

In the interest of clarity of exposition we will perform our mathematical analysis on a simplified system. Let $f_k:\mathbb{R}\to\mathbb{R}$, $k\in\mathcal{K}$, be a collection of bounded, Lipschitz continuous functions. We define the position process $\{X(t)\}_{t\geq 0}$ to be the pathwise solution to the following ODE:

$$\dot{X}(t)=\sum_{k\in\mathcal{K}} f_k(X(t))V_k(t), \tag{47}$$

where $\mathcal{K}\subset\mathbb{Z}$ is a finite collection of integers and $\{V_k(t)\}_{t\in\mathbb{R}}$ with $k\in\mathcal{K}$ is a collection of independent, almost surely continuous, stationary solutions to the GLE (4) with k-dependent coefficients a_k, b_k and c_k. Denote their respective ACFs by $\rho_k(t):=\mathbb{E}[V_k(t)V_k(0)]$.

Theorem 5.1. *Let $T>0$ be given and $\{V_k\}_{k\in\mathcal{K}}$ be defined as above. Then there exists a unique solution to (47) on the interval $[0,T]$ almost surely.*

Proof. Define Ω_c to be the probability one event that all velocity modes are continuous. That is to say, let

$$\Omega_c=\{\omega\in\Omega\,:\,V_k\in C(\mathbb{R}) \text{ for all } k\in\mathcal{K}\}. \tag{48}$$

For a given $\omega\in\Omega_c$ we can define the function

$$F(x,t;\omega)=\sum_{k\in\mathcal{K}} f_k(x)V_k(t;\omega). \tag{49}$$

Both F and $\frac{\partial F}{\partial x}$ are Lipschitz continuous in x and continuous in t for all $x,t\in\mathbb{R}$. By the Picard–Lindelöf Theorem, there exists a unique solution to the ODE

$$X(t;\omega)=F(X(t;\omega),t) \tag{50}$$

up to the time $T(\omega)\in(0,\infty]$ that the solution might blow up to positive or negative infinity.

To show that this does not happen in finite time, consider the following estimate which shows that for all deterministic $T > 0$, $\mathbb{E}\left[X^2(T)\right] < \infty$, implying that $P\{|X(T)| = \infty\} = 0$. Indeed,

$$\begin{aligned}
\mathbb{E}\left[X^2(T)\right] &= \mathbb{E}\left[\int_0^T \sum_k f_k(X(t))V_k(t)\mathrm{d}t \int_0^T \sum_j f_j(X(s))V_j(s)\mathrm{d}s\right] \\
&= \sum_k \sum_j \int_0^T \int_0^T \mathbb{E}\left[f_k(X(t))f_j(X(s))V_k(t)V_j(s)\right]\mathrm{d}s\mathrm{d}t \\
&\leq \sum_k \sum_j \int_0^T \int_0^T C_f^2\, \mathbb{E}\left[|V_k(t)V_j(s)|\right]\mathrm{d}s\mathrm{d}t \\
&\leq \sum_k \sum_j C_f^2 \int_0^T \int_0^T \mathbb{E}\left[V_k(t)^2\right]^{\frac{1}{2}} \mathbb{E}\left[V_j(s)^2\right]^{\frac{1}{2}} \mathrm{d}s\mathrm{d}t,
\end{aligned}$$

where C_f is a constant satisfying $C_f \geq f_k(x)$ for all $k \in \mathcal{K}$ and $x \in \mathbb{R}$, and we have used the finiteness of the number of terms in the sum and Cauchy–Schwarz.

By stationarity of the V_k's, the two factors in the integrand equal $\sqrt{\rho_k(0)}$ and $\sqrt{\rho_j(0)}$ respectively. It follows that

$$\mathbb{E}\left[X^2(T)\right] \leq \left(C_f\, T \sum_{k=1}^{K} \sqrt{\rho_k(0)}\right)^2. \qquad \square$$

5.2. Convergence of the numerical method

Let $T > 0$ be fixed and let $N \in \mathbb{N}$. Let $K_1 \leq K_2 \leq \ldots \leq K_N \leq \ldots \leq K$ be an increasing sequence of integers that converge to K. For each positive integer $k \leq K$ and $N \in \mathbb{N}$, we define the integrated increments of the noise process $\{u^n_{k,N}\}_{n\in\mathbb{Z}}$ to be jointly distributed as

$$u^n_{k,N} \sim \int_{t_n}^{t_{n+1}} V_k(t)dt$$

where $t_n = n/N$. We define an associated continuous time process

$$V_{k,N}(t) = \frac{u^n_{k,N}}{t_{n+1} - t_n}, \text{ for } t \in [t_n, t_{n+1}).$$

The numerical approximation analogous to (45) for the position process is then defined by $x^0_N = 0$, and

$$x^{n+1}_N = x^n_N + \sum_{k=1}^{K_N} f_k(x^n_N)u^n_{k,N}. \tag{51}$$

We define a continuous-time version of the numerical approximation to be

$$X_N(t) := x^n_N + \frac{(t - t_n)}{t_{n+1} - t_n} \sum_{k=1}^{K_N} f_k(x^n_N)u^n_{k,N} \text{ when } t \in [t_n, t_{n+1}). \tag{52}$$

We will demonstrate convergence of the numerical method in the following sense.

Theorem 5.2. *Let $T > 0$, and let $\{X(t)\}_{t\in[0,T]}$ be a solution to (47) with noises $\{V_k\}_{k\in\mathcal{K}}$ as defined in Theorem 5.1. Then $X_N(T) \to X(T)$ in distribution.*

Proof. We first define an intermediary process that can immediately be shown to converge to X in distribution and then use Slutsky's Theorem to complete the proof. To this end, for each ω such that the collection of V_k are continuous, define $\tilde{X}_N(\cdot, \omega)$ to be the solution of the ODE

$$\frac{\mathrm{d}}{\mathrm{d}t}\tilde{X}_N(t;\omega) = \sum_{k\in\mathcal{K}} f_k(\tilde{X}_N(t;\omega))V_{k,N}(t;\omega). \tag{53}$$

We claim $\tilde{X}_N$ converges to X in distribution. To see this, let $\Phi : C([0,T];\mathbb{R}^K) \to C([0,T];\mathbb{R})$ be the map defined by the ODE (47). That is to say, for an $\mathbb{R}^K$-valued function $V(t) = (V_1(t), V_2(t), \ldots, V_K(t))$, $X = \Phi(V)$ if X satisfies (47). Similarly, by (53), $\tilde{X}_N = \Phi(V_N(t))$ where $V_N(t) = (V_{1,N}(t), V_{2,N}(t), \ldots, V_{K,N}(t))$. Since the functions f_k are locally Lipschitz, the map Φ is continuous in the sup-norm. Since $V_N \to V$ in distribution, the continuous mapping theorem implies that $\tilde{X}_N \to X$ in distribution.

Now, define $\tilde{Y}_N(t) = X_N(t) - \tilde{X}_N(t)$. It remains to show that $\tilde{Y}_N(T) \to 0$ in probability. If we define $x_N(t) := x_N^n$ for $t \in [t_n, t_{n+1})$, then we can write $X_N(t)$ as an integral equation,

$$X_N(T) = \int_0^T \sum_{k=1}^{K_N} f_k(x_N(t))V_{k,N}(t)dt \tag{54}$$

It follows that

$$\begin{aligned}|\tilde{X}_N(T) - X_N(T)| &\le \int_0^T \sum_{k=1}^{K_N} |f_k(\tilde{X}_N(t)) - f_k(x_N(t))||V_{k,N}(t)|\mathrm{d}t + \int_0^T \sum_{k=K_N}^{K} |f_k(\tilde{X}_N(t))||V_{k,N}(t)|\mathrm{d}t \\ &\le \int_0^T \sum_{k=1}^{K_N} C_k\big(|\tilde{X}_N(t) - X_N(t)| + |X_N(t) - x_N(t)|\big)|V_{k,N}(t)|\mathrm{d}t + \int_0^t \sum_{k=K_N}^{K} |f_k(\tilde{X}_N(t))||V_{k,N}(t)|\mathrm{d}t'\end{aligned}$$

Here we have used the Lipschitz property of the f_k, $|f_k(x) - f_k(y)| \le C_k|x-y|$. If we take N sufficiently large, then because K is finite, we can take the last term to be zero. Defining $C_{Lip} = \max_k C_k$, with

$$\mathcal{V}_N(t) := C_{Lip}\sum_{k=1}^{K_N}|V_{k,N}(t)| \text{ and } I_N(t) := \int_0^t |X_N(t') - x_N(t')|\mathcal{V}_N(t)\mathrm{d}t$$

we observe that for each $\omega \in \Omega_c := \{\omega : X(t;\omega) \text{ is continuous for } t \in [0,T]\}$ we have

$$|\tilde{X}_N(T;\omega) - X_n(T;\omega)| \le I_N(T;\omega) + \int_0^T |\tilde{X}_N(t;\omega) - X_N(t;\omega)|\,\mathcal{V}_N(t;\omega)\mathrm{d}t.$$

It follows from the integral form of Gronwall's Inequality that

$$|\tilde{X}_N(T;\omega) - X_N(T;\omega)| \le I_N(T;\omega) + \int_0^T I_N(t;\omega)\mathcal{V}_n(t;\omega)\, e^{\int_t^T \mathcal{V}_N(s;\omega)\mathrm{d}s}\mathrm{d}t$$

Therefore, applying Cauchy–Schwarz to the second term,

$$\mathbb{E}\Big[|\tilde{X}_N(T) - X_N(T)|\Big] \le \mathbb{E}[I_N(T)] + \mathbb{E}\left[\int_0^T I_N^2(t)\mathrm{d}t\right]^{\frac{1}{2}} \mathbb{E}\left[\int_0^T \mathcal{V}_N^2(t)\, e^{2\int_t^T \mathcal{V}_N(s)\mathrm{d}s}\mathrm{d}t\right]^{\frac{1}{2}}. \tag{55}$$

For $t \in [t_n, t_{n+1})$, $\mathcal{V}_N(t) = \sum_{k=1}^{K}\sum_{i=1}^{n}|u_{k,N}^i/N|$. Noting that each of the summands is a Gaussian random variable, $\mathcal{V}_N(t)$ will have finite exponential moments, implying that the last factor in (55) is finite. Moreover, since $V_{N,k}(t)$ approaches the stationary process $V_N(t)$, the sequence of moments of $\mathcal{V}_N(t)$ is bounded in N.

It remains to show that $\mathbb{E}\left[\int_0^T I_N^2(t)\mathrm{d}t\right] \to 0$ as $N \to \infty$. Note first, by (52) we have for $t \in [t_n, t_{n+1})$ that

$$|X_N(t) - x_N(t)| \le (t - t_n)\sum_{k=1}^{K_N}|f_k(x_N(t))||V_{k,N}(t)| \le \frac{M}{N}\mathcal{V}_N(t)$$

where M is a constant such that $|f_k(x)| \le M$ for all $k \in \mathcal{K}$ and $x \in \mathbb{R}$ and we note that $t - t_n \le 1/N$ when $t \in [t_n, t_{n+1})$. Therefore

$$I_N^2(t) \le \frac{1}{N}\int_0^T M\mathcal{V}_N^2(t)\mathrm{d}t \qquad \square$$

Table 1
List of fixed parameters and dimensionless groups. The solvent is taken to be water and G_0 is chosen so that the polymer dynamic viscosity η_p is a hundred times that of water for a single Rouse kernel ($N = 1$).

Parameter	Symbol	Values	Units
Boltzmann cst x temp.	$k_B T$	4.1×10^{-9}	$\mu m^2\, mg\, ms^{-2}$
Solvent density	ρ	1×10^{-9}	$mg\, \mu m^{-3}$
Solvent dyn. viscosity	η_s	1×10^{-6}	MPa ms
Solvent kin. viscosity	$\nu_s = \eta_s/\rho$	1×10^{3}	$\mu m^2\, ms^{-1}$
Polymer mean stress	G_0	1×10^{-4}	$mg\, ms^{-2}$
Smallest relaxation time	τ_0	1	ms
Length	L	10	μm
Number of paths	N_p	1×10^{3}	
Characteristic time	$\theta = L^2/\nu_s$	0.1	ms
Characteristic velocity	$U = \sqrt{k_B T/\rho/L^3}$	6.32×10^{-2}	$\mu m\, ms^{-1}$
Reynolds number	$\mathrm{Re} = UL/\nu_s$	6.32×10^{-4}	
Beta parameter	$\beta = G_0 \rho L^2/\eta_s^2$	10	
Kappa parameter	$\kappa = \sqrt{k_B T \rho}/\eta_s$	2×10^{-3}	

Table 2
Polymer parameters for different numbers of kernels and $\alpha = 2$.

Number of kernels, N	$N = 1$	$N = 5$	$N = 50$	$N = 100$
Avg. rel. time $\tau_{\mathrm{avg},N}$ ms	1	7.32	8.13×10^{1}	1.64×10^{2}
Pol. dyn. viscosity $\eta_p = G_0 \tau_{\mathrm{avg},N}$ MPa ms	1×10^{-4}	7.32×10^{-4}	8.13×10^{-3}	1.64×10^{-2}
Pol. kin. viscosity $\nu_s = \eta_p/\rho\ \mu m^2\, ms^{-1}$	1×10^{5}	7.32×10^{5}	8.13×10^{6}	1.64×10^{7}

5.3. Parameter choices

We choose the following set of fundamental units: $[\mathtt{time}]$ = ms, $[\mathtt{length}]$ = μm, $[\mathtt{mass}]$ = mg. The corresponding units for force and pressure are: $[\mathtt{force}]$ = μN and $[\mathtt{pressure}]$ = MPa. The complete set of physical parameters are given in Table 1. We note that the Reynolds number is indeed small and we were justified in neglecting the nonlinear terms.

It has been recently demonstrated [11] that the iGLE with generalized Rouse kernel fits live data much better when the memory kernel has a high number of terms ($N \approx 200$) than for a low number of terms ($N \approx 5$). In order to span a range of dynamics, in our simulations we use the collection of values $N = 1,\ 5,\ 50$ and 100. It is important to note though that, as the number of terms in the generalized Rouse kernel changes, so does the average of the relaxation times. When it is important to emphasize this dependence, we introduce the notation $\tau_{\mathrm{avg},N}$ and observe that

$$\tau_{\mathrm{avg},N} = \frac{1}{N}\sum_{n=0}^{N} \tau_0 \Big(\frac{N}{N-n}\Big)^{\alpha} = N^{\alpha-1}\tau_0 \sum_{k=1}^{N} \frac{1}{k^{\alpha}}. \tag{56}$$

We see that $\lim_{N\to\infty} \tau_{\mathrm{avg,N}}/N^{\alpha-1} = \tau_0 \zeta(\alpha)$, where $\zeta(\alpha)$ is the Riemann zeta function. As a consequence, we are faced with a modeling decision in whether to hold the polymer viscosity η_p constant across the various values of N, or to hold the polymer mean stress $G_0 = \eta_p/\tau_{\mathrm{avg},N}$ constant. We chose to keep G_0 constant, which corresponds to keeping the coefficient of the memory-related terms in (25) constant. As a consequence, the only dimensionless group in the fluid equations is also constant: $\beta = G_0 \rho L^2/\eta_s^2 = 10$.

Regarding the shape parameter for the memory kernel, unless stated otherwise, we take $\alpha = 2$. For this case, the relaxation times and polymer parameters are summarized in Table 2.

5.4. Model validation

In order to compare to experimental data, we express the output of our model in terms of the empirical measures for two statistics:

$$\begin{aligned} &\textit{Ensemble MSD}: \quad M(t) = \mathrm{Var}\big(|\mathbf{X}(t) - \mathbf{X}(0))|\big) \\ &\textit{Ensemble Increment ACF}: \\ &A(n) = \frac{1}{M(t_1)^2}\mathrm{Cov}\Big(\big(\mathbf{X}(t_{n+1}) - \mathbf{X}(t_n)\big), \big(\mathbf{X}(t_1) - \mathbf{X}(0)\big)\Big). \end{aligned} \tag{57}$$

In the above, the lag times between t_{n+1} and t_n and t_1 and 0 are the same. As expected, particles advected by our model for a viscoelastic fluid exhibit some fundamental properties observed in live data [10,11]: sublinear behavior of the MSD

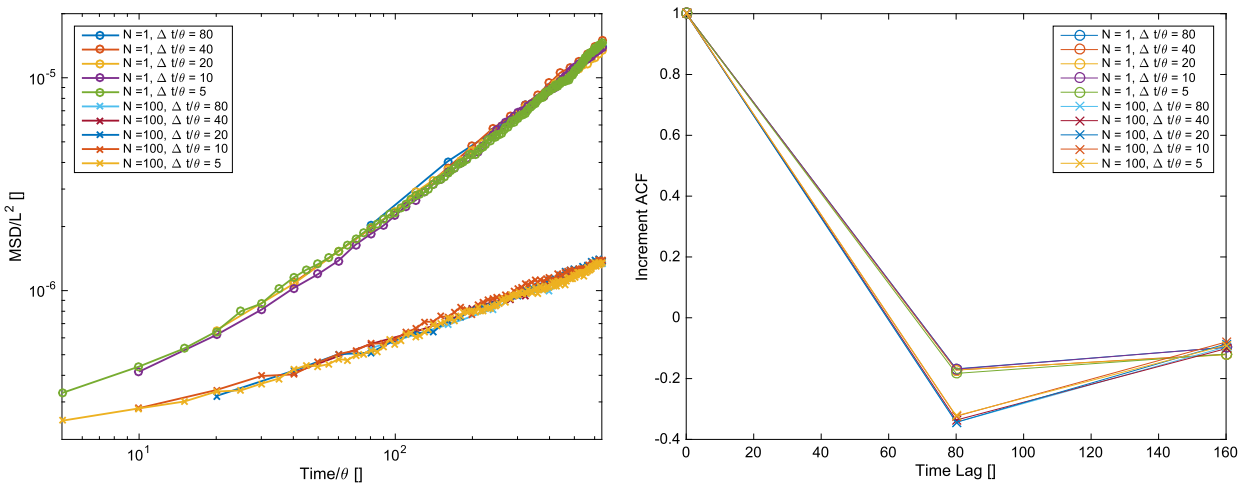

(a) Log-log MSD. (b) Increment ACF.

Fig. 2. Time convergence: (a) Dimensionless particle's MSD on a log–log scale as a function of dimensionless time and (b) dimensionless Increment ACF convergence of the particle's horizontal component as a function of dimensionless lag time for $\Delta t = 8$ ms, 4 ms, 2 ms, 1 ms and 0.5 ms for $N = 1$ (circles) and $N = 100$ (crosses). The parameters are $M = 256$, $T_{\text{final}} = 64$ ms, and $a = 1$ μm. All other parameters are given in Tables 1–2. We use the convention [] to denote a dimensionless variable in the labels.

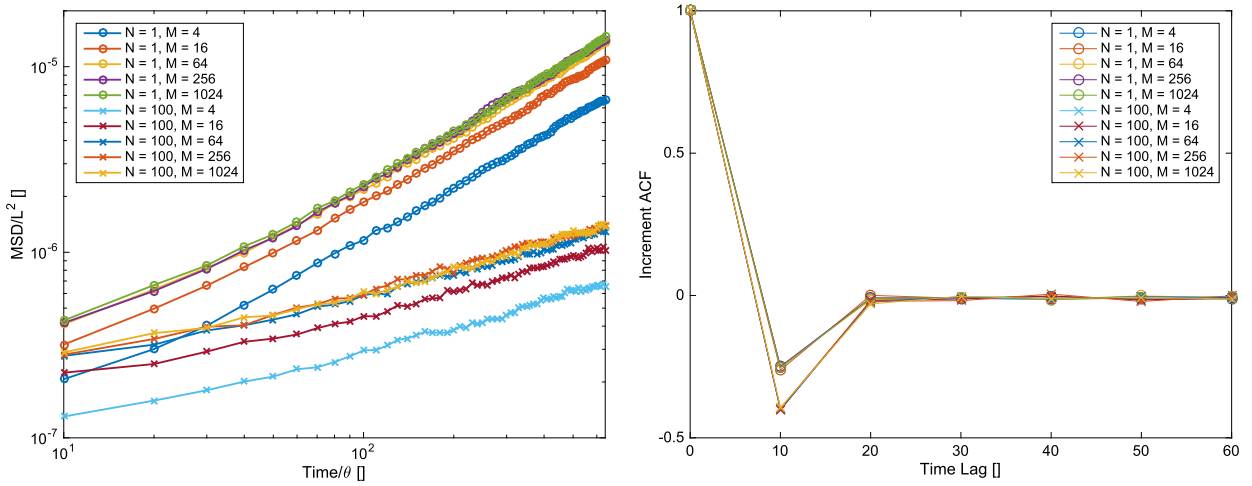

(a) Log-log MSD. (b) Increment ACF.

Fig. 3. Fourier convergence: (a) Dimensionless particle's MSD on a log–log scale as a function of dimensionless time and (b) dimensionless Increment ACF convergence of the horizontal component as a function of dimensionless lag time for $M = 4, 8, 16, 64, 256$ and 1024 for $N = 1$ (circles) and $N = 100$ (crosses). The parameters are $\Delta t = 1$ ms, $T_{\text{final}} = 64$ ms and $a = 1$ μm. All other parameters are given in Tables 1–2.

and first lag anti-correlation in the Increment ACF. Now we establish convergence of the numerical method and show that taking a non-dimensional time step $\Delta t/\theta = 10$ and $M = 256$ Fourier modes are sufficient to capture dynamics observed on experimental time scales.

Indeed, Fig. 2 shows the convergence in dimensionless time step for one kernel (circles) and one hundred kernels (crosses) with physical parameters given in Tables 1–2. In each case, we plot both $M(t)$ (a) and $A(n)$ of the horizontal component (b). We set $M = 256$, $T_{\text{final}}/\theta = 640$ (corresponding to 64 ms) and $a/L = 0.1$ (corresponding to 1 μm). The dimensionless time steps are 80, 40, 20, 10 and 5 corresponding to 8 ms, 4 ms, 2 ms, 1 ms and 0.5 ms. Taking the paths with $\Delta t/\theta = 5$ as the true solution, the absolute errors in the MSD at T_{final} are about 5×10^{-7} for $N = 1$ and 2×10^{-8} for $N = 100$, while the relative errors 4% and 2% respectively. From Fig. 2, we conclude that the method converges in time. Therefore, we pick $\Delta t/\theta = 10$ for the rest of this paper.

For the convergence of the simulation as a function of M, we again demonstrate it for one kernel (circles) and one hundred kernels (crosses) with the physical parameters given in Tables 1–2. In Fig. 3, we set $T_{\text{final}}/\theta = 640$ (corresponding to 64 ms), $a/L = 0.1$ (corresponding to 1 μm), and $\Delta t/\theta = 10$ (corresponding to 1 ms). We consider $M = 4, 16, 64, 256$ and 1024. Again, we plot both $M(t)$ (a) and $A(n)$ of the horizontal component (b). Taking the MSD with $M = 1024$ as the exact

Table 3
Absolute and relative error in the MSD at the final time (64 ms) for $N = 1$ and $N = 100$ corresponding to data plotted in Fig. 3.

Number of Fourier modes	$M = 4$	$M = 16$	$M = 64$	$M = 256$
Absolute error for $N = 1$	8×10^{-6}	4×10^{-6}	9×10^{-7}	6×10^{-7}
Absolute error for $N = 100$	7×10^{-7}	3×10^{-7}	8×10^{-8}	2×10^{-8}
Relative error for $N = 1$	54%	25%	6%	4%
Relative error for $N = 100$	52%	25%	6%	2%

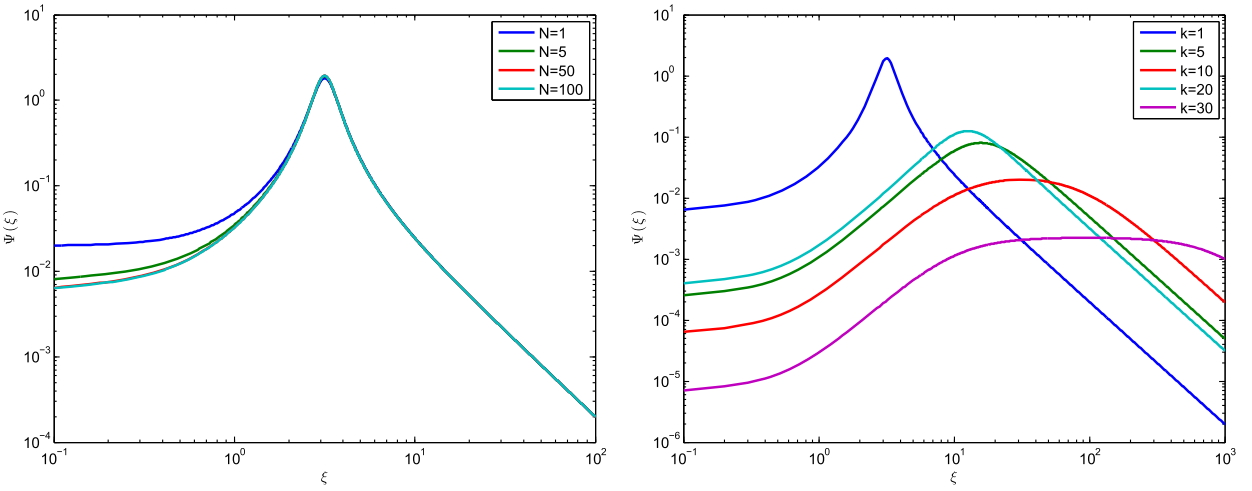

(a) $k = 1$. (b) $N = 50$.

Fig. 4. Log–log plot of $\Psi(\xi)$ for (a) $N = 1, 5, 50$ and 100 and (b) $k = 1, 5, 10, 20$ and 30.

solution, the absolute and relative errors at the final time for $N = 1$ and $N = 100$ are summarized in Table 3. We see that convergence in M is very rapid. Thus, we set $M = 256$ for the remainder of the simulations.

5.5. Behavior of the individual GLE modes of the fluid

As we will see in the next section, particle directly inherits certain properties of the fluid modes. In this section, we investigate the Fourier transform of the ACF of the fluid velocity modes, noting in particular the dependence on the associated wavevector $\mathbf{k}$.

Recall that for the GLEs that drive the fluid modes we have Eq. (4) with $a = k^2, b = \beta k^2$, and $c = \frac{1}{2\pi}$ where $k = |\mathbf{k}|$. First, we rewrite the Fourier transform $\widehat{\rho_Y}$ of the autocovariance function in a form similar to the one discussed in the proof of Proposition 2.1, letting $\widehat{\rho_Y}(\xi) = c^2\Psi(\xi)$ and $\Phi(x) = \frac{1}{N}\sum_{n=0}^{N-1}\frac{1}{x+\lambda_n}$ where $\lambda_n = \tau_n^{-1}$, $n = 0, \ldots, N-1$. Then we have

$$\Psi(\xi) = \frac{2a + 2b\mathrm{Re}(\Phi(i\xi))}{|i\xi + a + b\Phi(i\xi)|^2} = \frac{2}{k^2}\frac{1 + \beta\mathrm{Re}(\Phi(i\xi))}{|i\frac{\xi}{k} + 1 + \beta\Phi(i\xi)|^2}.$$

We note that the real and imaginary parts of $\Phi(i\xi)$ can be easily calculated, so that $\Psi(\xi)$ becomes

$$\Psi(\xi) = \frac{2}{k^2}\frac{1 + \beta\Phi_{\mathrm{real}}(\xi)}{(1 + \beta\Phi_{\mathrm{real}}(\xi))^2 + \left(\frac{\xi}{k} + \beta\Phi_{\mathrm{imag}}(\xi)\right)^2}$$

$$\Phi_{\mathrm{real}}(\xi) = \mathrm{Re}(\Phi(i\xi)) = \frac{1}{N}\sum_{n=0}^{N-1}\frac{\lambda_n}{\xi^2 + \lambda_n^2}$$

$$\Phi_{\mathrm{imag}}(\xi) = \mathrm{Im}(\Phi(i\xi)) = \frac{1}{N}\sum_{n=0}^{N-1}\frac{-\xi}{\xi^2 + \lambda_n^2}.$$

With these formulas in hand, we can directly analyze the behavior of the velocity autocovariance for small and large ξ. In particular, we note how its asymptotic behavior depends (or not) on k and N. For a visual guide, in Fig. 4, we plot $\Psi(\xi)$ on a log–log scale for (a) $N = 1, 5, 50$ and 100 and $k = 1$ and (b) $k = 1, 5, 10, 20$ and 30 and $N = 50$.

For the near zero behavior, utilizing the notation $\tau_{\mathrm{avg},N}$ introduced in Eq. (56), we have

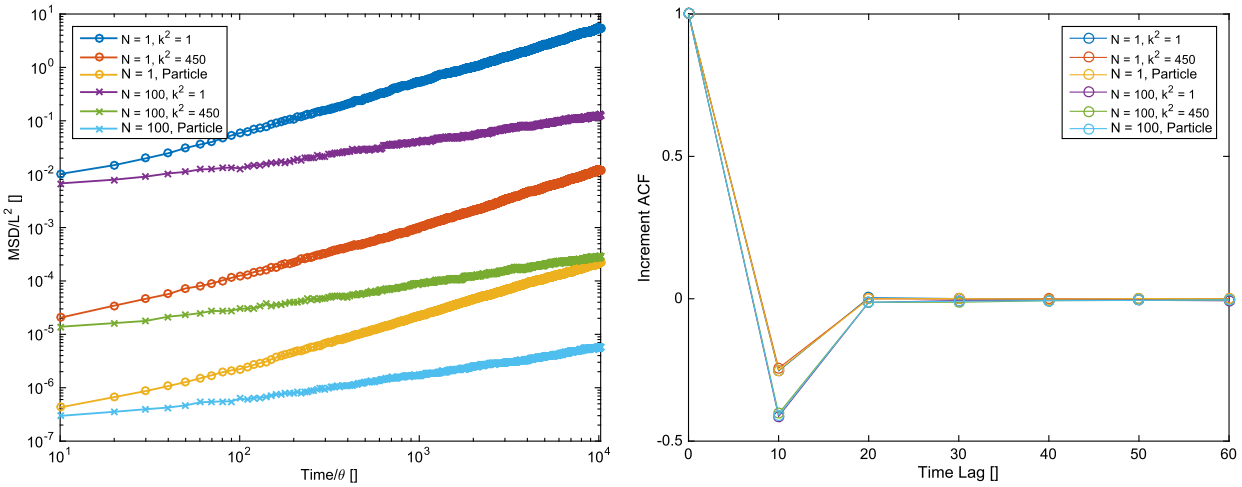

(a) Log-log MSD. (b) Increment ACF.

Fig. 5. Individual fluid GLEs: (a) Log–log plot of the MSD and (b) Increment ACF for individual fluid modes with $k^2 = 1$ and 450 and $N = 1$ and 100 compared with the particle's MSD and Increment ACF. The MSD depends on k, while the ACF does not.

$$\Psi(0;k,N) = \frac{2}{k^2}\frac{1}{1+\beta\tau_{\text{avg},N}}.$$

As seen in Fig. 4(b), $\lim_{k\to\infty}\Psi(0;k,N) = 0$. On the other hand, by (56) we have that $\tau_{\text{avg}} \sim N^{1-\alpha}$, so for fixed k, the value of $\Psi(0;k,N)$ decreases as N increases. This latter property has a direct consequence for the MSD of the associated iGLE. As pointed out in [48],

$$\lim_{t\to\infty}\frac{\mathbb{E}\left[Z^2(t)\right]}{t} = \lim_{\xi\to 0}\hat{\rho_Y}(\xi) = \frac{2c^2}{k^2}\frac{1}{1+\beta\tau_{\text{avg},N}}.$$

This behavior is displayed in Fig. 5(a) for $N = 1$ and $N = 100$. Note though, the Increment ACF does not depend on k, as is shown in Fig. 5(b). We comment more on this in the following section.

For large ξ, a direct computation shows that

$$\lim_{\xi\to\infty}\frac{\xi^2\Psi(\xi)}{2c^2k^2} = 1,$$

in other words, the tail of $\Psi(\xi)$ is independent of N and behaves as ξ^{-2} for large ξ. From Fig. 4(a), we remark that the location of the peak of $\Psi(\xi)$ is independent of N if $k = 1$. However, from Fig. 4(b) we see that, as k increases, the peak widens to a plateau.

5.6. Relating particle behavior to that of the fluid modes

As we have seen, the behavior of an immersed particle can be expressed in terms of a linear combination of the fluid modes (with coefficients that depend on the current position) as in Eq. (43). However, the nonlinear dependence on $X(t)$ prevents a explicit mathematical analysis of the MSD and ACF of immersed particles. To circumvent this issue in the viscous fluid case, Atzberger, Kramer and Peskin [26] introduced the following approximation for correlations in the fluid velocity field:

$$\mathbb{E}\left[\mathbf{u}(\mathbf{X}(t),t)\mathbf{u}(\mathbf{X}(0),0)\right] \overset{AKP}{\approx} \kappa^2\mathbb{E}\left[\mathbf{u}(\mathbf{0},t)\mathbf{u}(\mathbf{0},0)\right]. \tag{58}$$

Proceeding formally from (42) we can approximate the particle velocity ACF,

$$\mathbb{E}\left[\mathbf{V}(t)\mathbf{V}(0)\right] \approx \kappa^2\mathbb{E}\left[\mathbf{u}(\mathbf{X}(t),t)\mathbf{u}(\mathbf{X}(0),0)\right] \overset{AKP}{\approx} \kappa^2\mathbb{E}\left[\mathbf{u}(\mathbf{0},t)\mathbf{u}(\mathbf{0},0)\right].$$

Expressed in terms of Eq. (43), this takes the form

$$\mathbb{E}\left[\mathbf{V}(t)\mathbf{V}(0)\right] \overset{AKP}{\approx} 4\kappa^2\sum_{k\in\mathcal{K}^+}\mathbb{E}\left[\mathbf{v}_{\mathbf{k}}(t)\mathbf{v}_{\mathbf{k}}(0)\right]e^{-k^2a^2},$$

which can, in turn, be used to give an expression for the Increment ACF.

Let $\{t_n\}_{n\geq 0}$ be the times that we observe the position of a particle and assume that these time points are equally spaced. We introduce the following shorthand:

$$\Delta\mathbf{X}(n) := \mathbf{X}(t_{n+1}) - \mathbf{X}(t_n), \text{ and } \Delta\mathbf{U}_{\mathbf{k}}(n) := \mathbf{U}_{\mathbf{k}}(t_{n+1}) - \mathbf{U}_{\mathbf{k}}(t_n)$$

where $\mathbf{U}_{\mathbf{k}}(t) := \int_0^t \mathbf{v}_{\mathbf{k}}(s)\mathrm{d}s$.

Then, recalling the notation introduced in Eq. (57), under the assumption that the velocity process is stationary, we have

$$A(n) = \mathrm{Corr}\big(\Delta\mathbf{X}(n), \Delta\mathbf{X}(0)\big) = \frac{\mathrm{Cov}\big(\Delta\mathbf{X}(n), \Delta\mathbf{X}(0)\big)}{\mathrm{Var}\big(\Delta\mathbf{X}(0)\big)}.$$

Now,

$$\begin{aligned}
\mathrm{Cov}\big(\Delta\mathbf{X}(n), \Delta\mathbf{X}(0)\big) &= \mathbb{E}\left[\int_{t_n}^{t_{n+1}} \mathbf{V}(t)\mathrm{d}t \int_0^t \mathbf{V}(s)\mathrm{d}s\right] \\
&= \int_{t_n}^{t_{n+1}}\int_0^t \mathbb{E}[\mathbf{V}(t)\mathbf{V}(s)]\,\mathrm{d}s\mathrm{d}t \\
&\overset{AKP}{\approx} \int_{t_n}^{t_{n+1}}\int_0^t 4\kappa^2 \sum_{\mathbf{k}\in\mathcal{K}^+} \mathbb{E}[\mathbf{v}_k(t)\mathbf{v}_k(s)]\, e^{-k^2a^2}\mathrm{d}s\mathrm{d}t \\
&= 4\kappa^2 \sum_{\mathbf{k}\in\mathcal{K}^+} \mathrm{Cov}\big(\Delta\mathbf{U}_{\mathbf{k}}(n), \Delta\mathbf{U}_{\mathbf{k}}(0)\big)e^{-k^2a^2}.
\end{aligned}$$

Numerically, we have observed that the autocorrelation functions for the fluid modes appear to be independent of $\mathbf{k}$:

$$A_{\mathbf{k}}(n) := \mathrm{Corr}\big(\Delta\mathbf{U}_{\mathbf{k}}(n), \Delta\mathbf{U}_{\mathbf{k}}(0)\big) \approx a_n \in [-1, 1].$$

It follows from this and the preceding calculation that

$$\mathrm{Cov}\big(\Delta\mathbf{X}(n), \Delta\mathbf{X}(0)\big) \overset{AKP}{\approx} 4\kappa^2 \sum_{\mathbf{k}\in\mathcal{K}^+} a_n \mathrm{Var}\big(\Delta\mathbf{U}_{\mathbf{k}}(0)\big)e^{-k^2a^2} \approx a_n \mathrm{Var}\big(\Delta\mathbf{X}(0)\big)$$

where, in the last line, we have used the fact that $a_0 = 1$. Dividing both sides by $\mathrm{Var}\big(\Delta\mathbf{X}(0)\big)$, we have $A(n) \approx a_n$. That is to say, adopting the AKP approximation (58) and utilizing the numerical observation that $A_{\mathbf{k}}(n) \approx a_n$ is sufficient to explain the observation that the Increment ACF of the particle process matches that of the fluid modes.

5.7. A note on the length parameter a of the approximate δ function

It has been noted in multiple places that the length parameter that appears in δ_a (see Section 3.6) does not directly correspond to particle radius [49]. In fact, some authors have taken to calling the advected object a "blob" or "parcel" of fluid [23]. In this section, we show that there are two senses in which changes to a do not result in physically correct changes in particle tracking statistics. The first case has already been documented [50,51], namely that two dimensional stochastic fluid–particle simulations do not produce the Stokes–Einstein relationship between the diffusivity of a particle (which is proportional to the leading coefficient of the MSD) and the particle radius. Instead, for a purely viscous fluid, Donev and co-authors, [50,51], propose a logarithmic scaling of the diffusivity as a function of the radius of the form $c_1 \ln(L/(c_2 a))$, where $c_1 = k_B T/(4\pi\eta_s)$ is a physical constant and c_2 is a simulation dependent constant. In Fig. 6(a), we plot the particle's MSD for $N = 1$ (circles) and $N = 100$ (crosses) and $a = 0.5$ μm, 1 μm, 1.75 μm and 2 μm and clearly observe the dependence of the MSD on a in both cases. We then fit the logarithm of the MSD to the logarithm of the time by a linear polynomial and extract the diffusivity. Finally, we fit the obtained diffusivity to the logarithm of the inverse radius. Fig. 6(b) shows the diffusivity as a function of $1/a$ on a semi-log plot together with the linear fit. We observe that both the diffusivities and the resulting fits depend on N. This results is not surprising, since the polymeric viscosity (and thus the zero shear rate) viscosity changes between $N = 1$ and $N = 100$. We find for the constants $c_{1,N=1} = 6 \times 10^{-6}$, $c_{1,N=100} = 5 \times 10^{-6}$, $c_{2,N=1} = 0.16$, and $c_{2,N=100} = 0.65$. In Fig. 6, we set $T_{\text{final}} = 128$ ms, $M = 256$ and $\Delta t = 1$ μm and the other parameters as in Tables 1–2.

It has been proposed that one should introduce an empirical mapping between a and an effective particle radius [49]. However, such an approach will not work for our viscoelastic setting due to a second issue, which involves the relationship between particle radius and the magnitude of the anti-correlation in the first lag of the increment process. For particles diffusing in human mucus, Hill et al. [10] found that larger particles have a larger first step anti-correlation. However, we

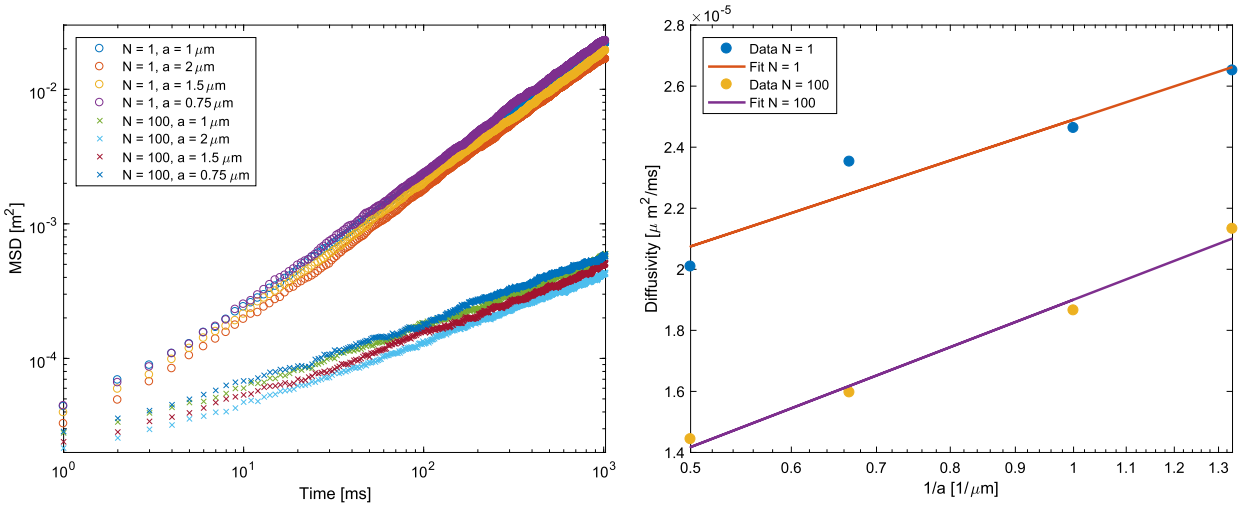

(a) Log-log MSD. (b) Semi-log diffusivity.

Fig. 6. Influence of a: (a) Particle's MSD on a log–log scale as a function of time and (b) diffusivity on a semi-log scale as a function of inverse radius for $a = 2$ μm, 1.5 μm, 1 μm and 0.75 μm and for $N = 1$ (circles) and $N = 100$ (crosses). The parameters are $M = 256$, $T_{\text{final}} = 128$ ms, and $\Delta t = 1$ ms. All other parameters are given in Tables 1–2.

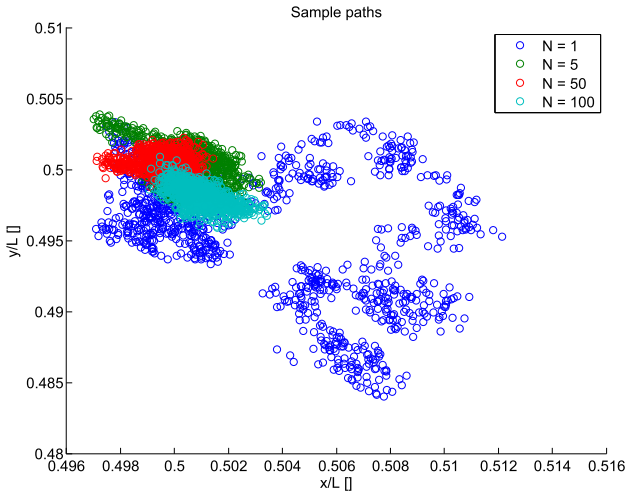

Fig. 7. Nondimensional sample path starting in the middle of the window for $N = 1, 5, 50$ and 100. The physical parameters are as in Tables 1 and 2. The simulation parameters are $\Delta t = 1$ ms, $T_{\text{final}} = 1024$ ms, and $M = 256$.

did not observe such a relationship in our simulations. In fact, changes in the parameter a seemed to have no effect on the Increment ACF at all. But in light of the preceding section, this should not be surprising. There, we showed that the particle Increment ACF looks exactly like the Increment ACF of the fluid modes, but these do not change with a because it does not even appear in their definition (see Section 3.4).

6. Discussion

We have introduced and analyzed a model for the movement of a thermally fluctuating particle in a linear viscoelastic fluid by generalizing the Landau–Lifschitz Navier–Stokes equations. Mimicking the procedure for generalizing the single-particle Langevin equation, we generalize the stress term of the fluid equation by way of integration against a memory kernel. Through non-dimensionalization and analysis of the relevant parameter regime, we show that the coefficient of the non-linear term is very small. We model a particle advected by the fluid by local averaging in the fluid velocity field and we numerically investigate simulations of particle trajectories.

Consistent with recent work, we use the generalized Rouse form for the memory function (see Eq. (8)). This is a three parameter family of functions that captures a cascade of linear response functions that act on N distinct time scales. When $N = 1$ this is called a Maxwell model, but recent statistical work has shown that much higher values of N are necessary to exhibit prominent viscoelastic effects [11]. For illustrative purposes, we plot in Fig. 7 a sample path for $N = 1, 5, 50$ and 100

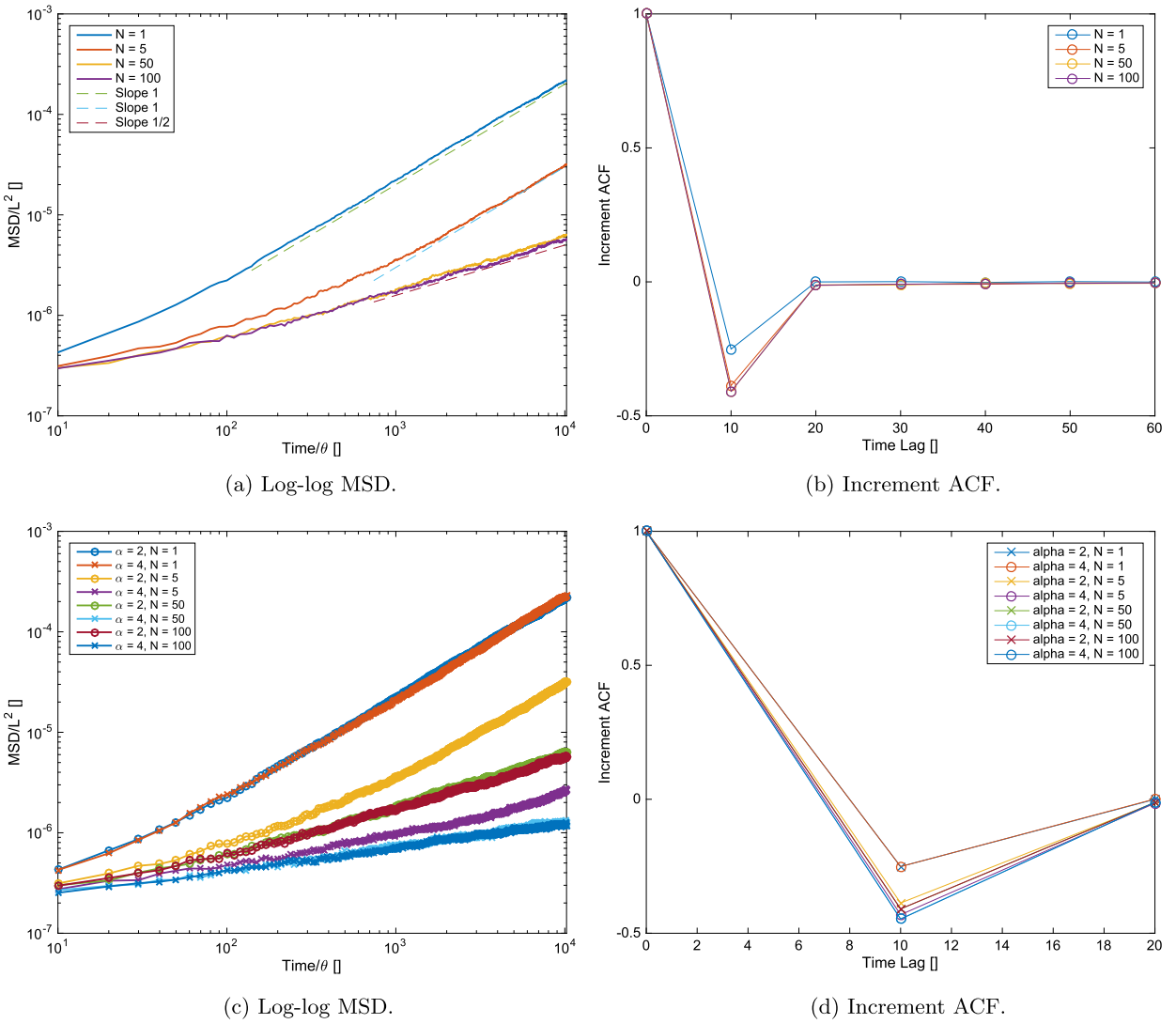

(a) Log-log MSD.

(b) Increment ACF.

(c) Log-log MSD.

(d) Increment ACF.

Fig. 8. Number of kernels and shape parameters: (a) Dimensionless MSD on a log–log scale as a function of dimensionless time, (b) dimensionless Increment ACF of the particle's horizontal component as a function of dimensionless lag time for $N = 1, 5, 50$ and 100, and similarly in (c)–(d) for memory kernel shape parameter $\alpha = 2$ and 4 for $N = 1, 5, 50$ and 100. The parameters are $M = 256$, $\Delta t = 1$ ms, $a = 1$ μm and $T_{\text{final}} = 1024$ ms. All other parameters are given in Tables 1–2.

starting in the middle of the window of width $L = 10$ μm. The physical parameters are as described in Tables 1–2, while the other parameters are $\Delta t = 1$ μs, $T_{\text{final}} = 1024$ ms, $M = 256$ (where M is the number of Fourier modes used to simulate the fluid) and $a = 1$ μm.

We analyze particle trajectories in terms of two statistics that are commonly used in particle tracking experiments: the mean-squared displacement of the particle position (MSD) and the auto-correlation function of increments of the position process (Increment ACF) (see definitions in Section 5.4). In Fig. 8, we plot both the particle MSD and the Increment ACF for $N = 1, 5, 50$ and 100 (a)–(b) and for $\alpha = 2$ and 4 (c)–(d). We set $T_{\text{final}} = 1024$ ms, $\Delta t = 1$ μm, $a = 1$ μm and $M = 256$. As expected, the statistics of the particle trajectories qualitatively match what is observed in the live data. Similar to the behavior of a single particle GLE, the behavior of particles advected by a viscoelastic fluid are mostly diffusive in character when N is small and subdiffusive when N is larger: in Fig. 8(a) we see that a line of slope one fits the log–log plot of the particle MSD for $N = 1$ and $N = 5$ quite well, but the particle MSD for $N = 100$ is better fit by slope $1/2$. Furthermore, as predicted by the more recent work [11], when the generalized Rouse kernel has shape parameter α, the corresponding particle MSD has exponent $1/\alpha$ (see Fig. 8(c). We note that this prediction is different from the one recorded in [52] because earlier versions of the model did not assume stationarity of the velocity process.

As discussed in the introduction, we investigated whether a central premise in the field of passive microrheology holds. Indeed, we find a strong connection between a particle's Increment ACF and that of the fluid modes, which indicates that recovery of the fluid's memory kernel from immersed particle dynamics should be possible in this model. It was not clear

from the outset of this project that this result would hold. It was known that the particle dynamics could be expressed as a sum over stationary fluid modes, but because definition of stochastic integro-differential equations that govern the modes depend on their "wave numbers" **k**, it appeared that the particle dynamics would be an average over a range of behaviors in the fluid modes. To our surprise, we found (Section 5.6) that the Increment ACF for the fluid modes are essentially identical. From this observation, along with an approximation (Eq. (58)) introduced by Atzberger, Kramer and Peskin [26], we can explain why memory effects in particle trajectories are so similar to that of the surrounding fluid (Section 5.6).

Though these results hold when particles are passively advected by the fluid, it is not yet clear how much the effect of particle inertia acting *back* on the fluid will change this. Consider, for example, that simulations using the stochastic IBM model for viscous fluids found *positive correlation* in the particle velocity ACF over small time intervals [26]. In generalizing to a fully coupled viscoelastic fluid–particle system, it is not at all clear how this feature will interact with the negative correlation we have observed at small times for passive advection. Any significant departure from the presently observed behavior could imperil our ability to recover fluid properties from particle statistics.

Implementing a fully coupled fluid–particle system remains a serious challenge though. Our method here relies on being able to exactly calculate the spectral density of the stationary processes from which our fluid is built. When particles are allowed to exert a force back on the fluid, then (1) the nonlinearity of the interaction prevents the derivation of an exact solution for the covariance function; and (2) Gaussianity itself is lost, meaning that more than two moments need to be considered. Overcoming these obstacles is left for future work.

In the mean time, the passive advection model features a number of interesting and important dynamics that still require satisfactory explanation. Most of these revolve around understanding the first step auto-correlation in the increment process. We have already discussed the surprise that the fluid mode Increment ACFs do not appear to depend on **k**. A further mystery appears in the Increment ACF plots (Fig. 8(d)). While, the model reliably matched expected behavior for the log–log slope of the MSD, the first step of the particle Increment ACF appears to be same for $\alpha = 2$ and $\alpha = 4$. This is different from what is observed in live data, for which anti-correlation in the first step increases as the subdiffusive exponent $(1/\alpha)$ decreases. Moreover, as we detail in Section 5.7, the first step of the particle Increment ACF does not depend on the parameter a in a way that is consistent with the interpretation of a as a particle radius. In live data, as particle radius increases, the first step anti-correlation becomes larger and the subdiffusive exponent decreases. It remains to be seen how or if these properties change when particle inertia is allowed to act back on the fluid, but issues with the scaling of a have long been documented in the implementation of the stochastic IBM for viscous fluids. Developing a model that can faithfully handle multiple particle sizes in the same fluid might ultimately require a change in coarse-graining philosophy.

Acknowledgements

The authors would like to thank M. Gregory Forest, Peter Kramer, and Aleksandar Donev for several helpful conversations in the development of this work. The authors were supported by NSF-DMS 1412998.

References

[1] C. Storm, J.J. Pastore, F. MacKintosh, T. Lubensky, P.A. Janmey, Nonlinear elasticity in biological gels, Nature 435 (2005) 191–194.
[2] G. Massiera, K.M. Van Citters, P.L. Biancaniello, J.C. Crocker, Mechanics of single cells: rheology, time dependence, and fluctuations, Biophys. J. 93 (10) (2007) 3703–3713.
[3] S.K. Lai, Y.-Y. Wang, D. Wirtz, J. Hanes, Micro- and macrorheology of mucus, Adv. Drug Deliv. Rev. 61 (2) (2009) 86–100.
[4] J.N. Wilking, T.E. Angelini, A. Seminara, M.P. Brenner, D.A. Weitz, Biofilms as complex fluids, Mater. Res. Soc. Bull. 36 (05) (2011) 385–391.
[5] M. Weiss, M. Elsner, F. Kartberg, T. Nilsson, Anomalous subdiffusion is a measure for cytoplasmic crowding in living cells, Biophys. J. 87 (5) (2004) 3518–3524.
[6] I. Tolić-Nørrelykke, E.-L. Munteanu, G. Thon, L. Oddershede, K. Berg-Sørensen, Anomalous diffusion in living yeast cells, Phys. Rev. Lett. 93 (7) (2004) 078102.
[7] I. Golding, E. Cox, Physical nature of bacterial cytoplasm, Phys. Rev. Lett. 96 (9) (2006) 098102.
[8] I. Bronstein, Y. Israel, E. Kepten, S. Mai, Y. Shav-Tal, E. Barkai, Y. Garini, Transient anomalous diffusion of telomeres in the nucleus of Mammalian cells, Phys. Rev. Lett. 103 (1) (2009) 018102.
[9] S.C. Weber, A.J. Spakowitz, J.A. Theriot, Bacterial chromosomal loci move subdiffusively through a viscoelastic cytoplasm, Phys. Rev. Lett. 104 (23) (2010) 238102.
[10] D.B. Hill, P.A. Vasquez, J. Mellnik, S.A. McKinley, A. Vose, F. Mu, A.G. Henderson, S.H. Donaldson, N.E. Alexis, R.C. Boucher, M.G. Forest, A biophysical basis for mucus solids concentration as a candidate biomarker for airways disease, PLoS ONE 9 (2) (2014) e87681.
[11] M. Lysy, N.S. Pillai, D.B. Hill, M.G. Forest, J.W. Mellnik, P.A. Vasquez, S.A. McKinley, Model comparison and assessment for single particle tracking in biological fluids, J. Am. Stat. Assoc. 111 (516) (2016) 1413–1426.
[12] A. Donev, J. Bell, A. Garcia, B. Alder, A hybrid particle-continuum method for hydrodynamics of complex fluids, Multiscale Model. Simul. 8 (3) (2010) 871–911.
[13] P. Atzberger, Incorporating shear into stochastic eulerian lagrangian methods for rheological studies of complex fluids and soft materials, Physica D 265 (2013) 57–70.
[14] R. Kubo, The fluctuation–dissipation theorem, Rep. Prog. Phys. 29 (1) (1966) 255.
[15] T. Mason, D. Weitz, Optical measurements of frequency-dependent linear viscoelastic moduli of complex fluids, Phys. Rev. Lett. 74 (7) (1995) 1250–1253.
[16] T. Indei, J.D. Schieber, A. Córdoba, E. Pilyugina, Treating inertia in passive microbead rheology, Phys. Rev. E 85 (2) (2012) 021504.
[17] H.M. Schaink, J.J.M. Slot, R.J.J. Jongschaap, J. Mellema, The rheology of systems containing rigid spheres suspended in both viscous and viscoelastic media, studied by Stokesian dynamics simulations, J. Rheol. 44 (3) (2000) 473–498.
[18] A. Levine, T. Lubensky, Two-point microrheology and the electrostatic analogy, Phys. Rev. E 65 (1) (2001) 011501.

[19] L. Starrs, P. Bartlett, One- and two-point microrheology of viscoelastic media, J. Phys. Condens. Matter 15 (2003) S251.
[20] C. Hohenegger, M.G. Forest, Two-bead microrheology: modeling protocols, Phys. Rev. E (2008) 031501.
[21] A. Donev, J. Bell, A. de la Fuente, A. Garcia, Diffusive transport by thermal velocity fluctuations, Phys. Rev. Lett. 106 (20) (2011) 204501.
[22] P. Atzberger, Stochastic eulerian lagrangian methods for fluid structure interactions with thermal fluctuations, J. Comput. Phys. 230 (2011) 2821–2837.
[23] F.B. Usabiaga, R. Delgado-Buscalioni, B.E. Griffith, A. Donev, Inertial coupling method for particles in an incompressible fluctuating fluid, Comput. Methods Appl. Mech. Eng. 269 (2014) 139–172.
[24] P. Atzberger, Velocity correlations of a thermally fluctuating brownian particle: a novel model of the hydrodynamic coupling, Phys. Lett. A 351 (2006) 225–230.
[25] P. Atzberger, A note on the correspondence of an immersed boundary method incorporating thermal fluctuations with Stokesian–Brownian dynamics, Phys. D, Nonlinear Phenom. 226 (2) (2007) 144–150.
[26] P. Atzberger, P. Kramer, C. Peskin, A stochastic immersed boundary method for fluid–structure dynamics at microscopic length scales, J. Comput. Phys. 224 (2) (2007) 1255–1292.
[27] P. Kramer, C. Peskin, P. Atzberger, On the foundations of the stochastic immersed boundary method, Comput. Methods Appl. Mech. Eng. 197 (25–28) (2008) 2232–2249.
[28] S. Delong, F.B. Usabiaga, A. Donev, Brownian dynamics of confined rigid bodies, J. Chem. Phys. 143 (2015) 144107.
[29] T.G. Mason, D.A. Weitz, Optical measurements of frequency-dependent linear viscoelastic moduli of complex fluids, Phys. Rev. Lett. 74 (7) (1995) 1250–1253.
[30] T.G. Mason, Estimating the viscoelastic moduli of complex fluids using the generalized Stokes–Einstein equation, Rheol. Acta 39 (2000) 371–378.
[31] T.M. Squires, T.G. Mason, Fluid mechanics of microrheology, Annu. Rev. Fluid Mech. 42 (2010) 413–438.
[32] S.C. Kou, Stochastic modeling in nanoscale biophysics: subdiffusion within proteins, Ann. Appl. Stat. (2008) 501–535.
[33] J. Fricks, L.Y. Yao, T.C. Elston, M.G. Forest, Time domain methods for passive microrheology and anomalous diffusive transport in soft matter, SIAM J. Appl. Math. 69 (2009) 1277–1308.
[34] S.A. McKinley, L. Yao, M.G. Forest, Transient anomalous diffusion of tracer particles in soft matter, J. Rheol. 53 (6) (2009) 1487–1506.
[35] P.E. Rouse Jr, A theory of the linear viscoelastic properties of dilute solutions of coiling polymers, J. Chem. Phys. 21 (1953) 1272.
[36] R. Kupferman, Fractional kinetics in Kac–Zwanzig heat bath models, J. Stat. Phys. 114 (1–2) (2004) 291–326.
[37] S.C. Kou, Stochastic modeling in nanoscale biophysics: subdiffusion within proteins, Ann. Appl. Stat. 2 (2) (2008) 501–535.
[38] C. Hohenegger, On equipartition of energy and integrals of Generalized Langevin Equations with generalized Rouse kernel, Commun. Math. Sci. 15 (2) (2017) 539–554.
[39] S. Asmussen, P.W. Glynn, Stochastic Simulation: Algorithms and Analysis, vol. 57, Springer, 2007.
[40] L.P. Pitaevskii, E.M. Lifshitz, Statistical Physics, Part 2, Course of Theoretical Physics, vol. 9, Butterworth–Heinemann, 1980.
[41] R.G. Larson, Constitutive Equations for Polymer Melts and Solutions, Butterworth–Heinemann, 1988.
[42] K. Xu, M. Forest, I. Klapper, On the correspondence between creeping flows of viscous and viscoelastic fluids, J. Non-Newton. Fluid Mech. 145 (2–3) (2007) 150–172.
[43] J.D. Ferry, Viscoelastic Properties of Polymers, John Wiley & Sons, 1980.
[44] C. Gardiner, Stochastic Methods: A Handbook for the Natural and Social Sciences, 4th edition, Springer, 2009.
[45] D.T. Gillespie, Exact numerical simulation of the Ornstein–Uhlenbeck process and its integral, Phys. Rev. E 54 (2) (1996) 2084.
[46] M. Richardson, L.N. Trefethen, A sinc function analogue of chebfun, SIAM J. Sci. Comput. 33 (5) (2011) 2519–2535.
[47] T.A. Driscoll, N. Hale, L.N. Trefethen (Eds.), Chebfun Guide, Pafnuty Publications, 2014.
[48] G. Didier, S.A. McKinley, D.B. Hill, J. Fricks, Statistical challenges in microrheology, J. Time Ser. Anal. 33 (5) (2012) 724–743.
[49] T.T. Bringley, Analysis for the Immersed Boundary Method for Stokes Flow, Ph.D. thesis, New York University, 2008.
[50] F.B. Usabiaga, X. Xie, R. Delgado-Buscalioni, A. Donev, The Stokes–Einstein relation at moderate Schmidt number, J. Chem. Phys. 139 (21) (2013) 214113.
[51] A. Donev, T.G. Fai, E. Vanden-Eijnden, A reversible mesoscopic model of diffusion in liquids: from giant fluctuations to Fick's law, J. Stat. Mech. Theory Exp. 2014 (4) (2014) P04004.
[52] S.A. McKinley, L. Yao, M.G. Forest, Transient anomalous diffusion of tracer particles in soft matter, J. Rheol. 53 (6) (2009) 1487–1506.